IEEE Access
Multidisciplinary | Rapid Review | Open Access Journal

Received 1 July 2024, accepted 1 August 2024, date of publication 6 August 2024, date of current version 26 August 2024.

Digital Object Identifier 10.1109/ACCESS.2024.3439414

RESEARCH ARTICLE

Distributed Robust Adaptive Control for Finite-Time Flight Formation of Multi-Quadcopter Systems With Large Lumped Uncertainties

LUIS F. CANAZA CCARI[1], PABLO RAUL YANYACHI[1,2], (Senior Member, IEEE), JUAN C. CUTIPA LUQUE[1,2], (Member, IEEE), AND DANIEL YANYACHI[1,2]

[1]Instituto de Investigación Astronómico y Aeroespacial Pedro Paulet, Universidad Nacional de San Agustín de Arequipa, Arequipa 04000, Peru
[2]Department of Electronic Engineering, Universidad Nacional de San Agustín de Arequipa, Arequipa 04000, Peru

Corresponding author: Pablo Raul Yanyachi (raulpab@unsa.edu.pe)

ABSTRACT This article presents a new robust formation control approach for a system of multiple Quadcopter Unmanned Aerial Vehicle (QUAV) in complex and challenging flight scenarios with large lumped uncertainties. The aim is to achieve fast convergence to the desired formation pattern, high tracking accuracy, and solid robustness. To this end, a novel finite-time nonlinear control strategy, Adaptive Backstepping Recursive Integral Non-singular Fast Terminal Sliding Mode Control (ABRINFTSMC), is designed. The formation control system of each QUAV, based on ABRINFTSMC, is divided into an underactuated position subsystem for the outer loop and a fully actuated attitude subsystem for the inner loop. A Robust Finite-Time Distributed Consensus Formation Control Protocol (RFDCFCP) is developed for the outer loop to ensure the convergence of the aircraft to the desired formation pattern in a finite time and maintain its alignment throughout the flight mission. For the inner loop, a Robust Finite-Time Attitude Stabilization Control (RFASC) is developed to allow the aircraft to track the desired attitude generated by the outer loop in a finite time. The stability of the closed-loop system is rigorously analyzed using Lyapunov theory to ensure convergence of all formation tracking errors to the origin in finite time. Finally, numerical simulations are performed under different scenarios to validate the performance of the proposed method, and a comprehensive comparative study with recent formation control approaches is carried out. The results confirm that the proposed formation control exhibits superior performance regarding fast convergence, tracking accuracy, and robustness, crucial features for multi-QUAV system flight formation.

INDEX TERMS Distributed formation control, multi-UAV system, nonlinear control, quadcopter.

I. INTRODUCTION

A. CONTEXT AND MOTIVATIONS

In recent years, research on formation control of multiple Quadcopter Unmanned Aerial Vehicles (QUAVs) has experienced significant growth in the field of aerospace and control engineering due to their diverse applications in society, such as cooperative transport of suspended loads [1], [2], mapping and inspection of large terrain areas [3], [4], and search and rescue operations [5], [6], among others. This interest is due to the distinctive characteristics of quadcopters as aerial vehicles, which include their flexible flight capability, small size, and fast maneuverability [7], [8]. Therefore, a group of QUAVs can efficiently collaborate on complex flight missions, thereby reducing the complexity inherent in sophisticated tasks and improving efficiency and

The associate editor coordinating the review of this manuscript and approving it for publication was Xiwang Dong.

effectiveness, resulting in increased accuracy and coverage compared to a single aerial vehicle.

With the increasing demand for control of multiple QUAVs, developing effective flight formation control systems is crucial. However, the development of these control systems poses significant challenges for researchers. In general, controlling a single QUAV is a difficult task due to its nonlinear, highly coupled, and underactuated dynamics with six degrees of freedom and only four control actions [9], [10], [11]. Moreover, in practical situations, quadcopter aircraft are subject to considerable and unknown uncertainties, such as wind gusts, unmodeled internal dynamics, and variations in vehicle parameters [12], [13]. Controlling multiple QUAVs to achieve a common goal is even more complex. These difficulties stem from the control design methodology, the communication between all agents, the risk of collisions, and the inherent complexity of quadcopter dynamics [14], [15], [16]. Therefore, controlling a multi-QUAV system requires an advanced, reliable and robust control strategy to address the issues encountered and achieve high performance in flight formation stability. This strategy must meet fundamental criteria, such as fast convergence to the desired formation pattern, accuracy in tracking the reference trajectory, and solid robustness against large lumped uncertainties, key features in multiple QUAVs formation control [16], [17].

In this research, a novel flight formation control strategy that combines nonlinear advancing control theories with an adaptive gain adjustment method is designed. The main objective of this study is to address the problem of formation control of a multi-QUAV system by simultaneously achieving fast convergence, high tracking accuracy, and solid robustness, all within the same formation control framework.

B. REVIEW OF THE STATE OF THE ART ON THE CONTROL OF MULTIPLE QUADCOPTERS

Several advanced control approaches have been proposed in the scientific literature to address the flight formation of a multi-QUAV system. For example, in [18], a specific backstepping control scheme was developed for this application. Subsequent research, such as [19], also employed backstepping control theory to design a robust distributed formation control system using a leader-follower scheme. In [20], a self-triggering sliding mode control was implemented to achieve the distributed formation of a group of QUAVs, using graph theory to manage the communication between the agents. In turn, [21] proposed a cooperative formation control based on a leader-follower scheme, using a fractional sliding mode control strategy and the potential field algorithm. More recent work [22] combined the backstepping and sliding mode control theories to develop a robust formation flight control scheme, further integrating a neural network with radial basis function to mitigate external disturbances.

Previous research works [18], [19], [20], [21], [22] focused on the formation control of a multi-QUAV system using various advanced control approaches. However, these works presented asymptotic stability, resulting in a slow convergence of the states to the equilibrium point, with an unpredictable settling time that cannot be estimated or adjusted. This characteristic makes them less suitable for practical applications, where fast convergence to the desired formation pattern is crucial in the formation control of multi-QUAV systems [16], [17]. Moreover, approaches [20], [21], [22] used conventional sliding surfaces that may suffer from chattering phenomena, which could cause instability and affect the performance of the control system in complex flight missions. To overcome these limitations, the scientific literature has investigated advanced control approaches with finite-time stability, which aim to improve the formation control performance and achieve fast convergence to the desired formation pattern.

C. RELATED WORK

In recent years, the design of finite-time formation control approaches has been widely investigated in the literature in multi-agent systems, including mobile robots [23], [24], underwater robots [25], [26], and quadcopters [27], [28], [29], [30], [31], [32], [33], [34], [35]. In the field of multi-QUAV system formation control, a distributed formation control methodology with online learning capability using neural networks was proposed in [27]. However, this work focused only on finite-time control for the rotational dynamics of QUAVs, without considering finite-time control for the complete system dynamics; moreover, external disturbances in flight formation were ignored. In work [28], a distributed consensus control approach was designed using a continuous adaptive non-singular terminal sliding mode control strategy. In [29], a leader with dynamic input was considered to develop a finite-time distributed tracking formation protocol employing second-order sliding mode control. Although these works, [28], [29] addressed finite-time control for full quadcopter dynamics, like [27], they did not consider external disturbances and unknown uncertainties in the aircraft dynamic system, which does not guarantee the robustness of the proposed control approaches to unknown uncertainties and external disturbances.

On the other hand, in [30], a formation control approach with a leader-follower structure was presented using backstepping control theory to design finite-time distributed control algorithms for QUAVs position and attitude. In [31], a new finite-time control scheme was proposed by designing a distributed formation control strategy based on a sliding-mode variable surface for the position system and a fast terminal sliding mode control strategy for the attitude system. The work [32] introduced a formation control scheme based on a finite-time convergent extended state observer to improve the disturbance rejection capability and flight formation tracking performance. Based on [32], the authors in [33] combined a fast terminal sliding mode control strategy with a disturbance observer to form a robust finite-time formation control framework. In the recent work [34],

a distributed robust formation control strategy based on sliding mode control theory was developed for a group of heterogeneous quadcopters characterized by different physical parameters. In the most recent study [35], the authors developed a novel fixed/finite-time sliding mode control strategy that employs Taylor series expansion to predict subsequent sliding surface responses and achieve an optimal formation control law.

Although finite-time formation control approaches [30], [31], [32], [33], [34], [35] have achieved interesting results in terms of convergence speed and have considered external disturbances in quadcopter dynamical systems, it is crucial to highlight some limitations. These works did not consider other types of uncertainties, such as unmodeled internal dynamics or variations of aircraft physical parameters. In addition, the external disturbances considered in these investigations were limited in magnitude without addressing more realistic and significant external disturbances. In a real flight scenario, QUAVs are subject to large lumped uncertainties, such as wind gusts, modeling uncertainties, and parametric uncertainties. These conditions must be carefully considered in the design of formation control systems to ensure robust and reliable performance in challenging flight environments.

Based on the state-of-the-art review of multi-QUAV flight formation control approaches, there is a clear need for further efforts in designing more advanced control methods that can deal with large uncertainties lumped in complex flight scenarios and simultaneously achieve properties of fast convergence, high tracking accuracy, and solid robustness. Motivated by this need, we propose a novel finite-time nonlinear control strategy in this research that combines advanced control theories of sliding mode and backstepping with a robust adaptive gain tuning method. This approach is designed to address the above mentioned challenges and achieve an efficient distributed formation control system in complex and challenging flight scenarios.

D. CONTRIBUTIONS

The main contributions of this research are the following:

- A novel nonlinear control strategy called Adaptive Backstepping Recursive Integral Non-singular Fast Terminal Sliding Mode Control (ABRINFTSMC) is designed to address the formation control problem of a multi-QUAV system. Based on this proposed strategy, the following schemes are developed for the formation control system of each QUAV: a Robust Finite-Time Distributed Consensus Formation Control Protocol (RFDCFCP) for the underactuated position subsystem and a Robust Finite-Time Attitude Stabilization Control (RFASC) for the fully actuated attitude subsystem. In addition, the finite-time stability of the ABRINFTSMC control strategy is demonstrated through an extensive theoretical analysis using Lyapunov theory and mathematical lemmas.
- In contrast to robust formation control approaches [30], [31], [32], [33], [34], [35], which consider only external disturbances with limited magnitude, this research addresses large lumped uncertainties, similar to those that a multi-QUAV system would face in a real flight scenario. These uncertainties include external disturbances such as wind gusts, variations in physical parameters, and unmodeled internal dynamics. As a result, the proposed approach offers greater adaptability and robustness to complex scenarios with realistic lumped uncertainties, making it more suitable for practical implementation.
- The viability and effectiveness of the proposed control method are validated through numerical simulations, compared with recent formation control approaches such as Distributed Robust Formation Control (DRFC) [34] and Predictor-based Constrained Fixed-time Sliding Mode Control (PCFSMC) [35]. The results obtained, supported by quantitative comparative analysis, highlight the advantages and superiority of the proposed approach in terms of fast convergence, tracking accuracy, and robustness, which are key features of the flight formation of a multi-QUAV system.

E. MANUSCRIPT ORGANIZATION

Section II presents the preliminaries for the control design. Section III develops the mathematical model of the multi-QUAV system. In Section IV, the formation control is designed. The finite time stability is demonstrated in section V. The results of this investigation are presented in section VI. Finally, the conclusions of the research are presented in section VII.

II. PRELIMINARIES

This section presents some mathematical concepts and lemmas necessary for the design of the formation controller and the finite-time stability analysis.

A. GRAPH THEORY

This study employs a leader-follower scheme to address the formation control of multi-QUAV, with one leader (indexed as 0) and N followers. Graph theory, widely used in multi-agent systems, defines the communication topology between the quadcopters.

Consider a group of N quadcopter agents communicating with their neighbors described by the graph $G = (V, E)$, where V and E represent the nodes and edges, respectively. An edge (V_i, V_j) means that quadcopter agent i can access the information of quadcopter agent j and vice versa. The adjacency matrix of a graph is defined as A, whose elements are $a_{ij} > 0$ if $(V_i, V_j) \in E$ and $a_{ij} = 0$ otherwise. The degree matrix is defined as $D = \text{diag}(d_1, \ldots, d_N) \in \mathbb{R}^{N\times N}$ with $d_i = \sum_{j=1}^{N} a_{ij}$. Then, the Laplacian matrix can be expressed as $L = D - A$. Consider a diagonal matrix $B = \text{diag}(b_1, \ldots, b_N)$ that describes the interconnection of the data flow from the leader to the followers, where $b_i > 0$ if

the leader agent shares its information with the follower agent i; otherwise, $b_i = 0$.

B. DEFINITIONS AND LEMMAS

Definition 1 ([12] (Finite-time stability)): Consider the nonlinear system:

$$\dot{x} = f(x), \quad x(0) = x_0, \tag{1}$$

where $x \in \mathbb{R}^n$, and the nonlinear function $f : D \to \mathbb{R}^n$ is continuous on an open neighborhood of the origin $D \subseteq \mathbb{R}^n$. The origin $x = 0$ is a finite-time global convergent equilibrium of the nonlinear system (1) if it is globally asymptotically stable. There is an open neighbourhood $U \subseteq D$ of the origin and a function $T_x : U\backslash\{0\} \to (0, \infty)$ such that each solution $x(t, x_0)$ of the nonlinear system (1) starting from the initial point $x_0 \in U\backslash\{0\}$ is well defined for $t \in [0, T_x(x_0))$, and $\lim_{t\to T_x(x_0)} x(t, x_0) = 0$. $T_x(x_0)$ is defined as the function of the convergence time, i.e., the settling time (for x_0). The origin is a finite-time stable equilibrium if it is finite-time convergent and Lyapunov stable. If $U = D = \mathbb{R}^n$, the origin is said to be a globally stable equilibrium in finite time.

Lemma 1 ([36]): Suppose there exists a positive definite Lyapunov function $V(x(t)) : \mathbb{R}^n \to \mathbb{R}$, and its derivative satisfies $\dot{V}(x) \leq -L_V V^{\Pi} + F_V$, where $L_V > 0, 0 < \Pi < 1$ and $F_V > 0$ are positive definite constants, then the origin of system (1) is stable in finite time for $\forall 0 < \varrho < 1$, when the settling time is given by:

$$T_f = \frac{1}{(1-\Pi)\varrho L_V}\left(V^{1-\Pi}(x(0)) - \left(\frac{F_V}{(1-\varrho)L_V}\right)^{\frac{1-\Pi}{\Pi}}\right). \tag{2}$$

Lemma 2 ([37]): For any Lyapunov function that verifies the following inequality $\dot{V}(x) \leq -\varpi_1 V - \varpi_2 V^{\Pi}$, where the constants $\varpi_1 > 0, \varpi_2 > 0, 0 < \Pi < 1$, there exists a finite time stability so that the settling time is given by:

$$T_f \leq \frac{1}{(1-\Pi)\varpi_1}\ln\left(\frac{\varpi_1 V^{1-\Pi}(x(0)) + \varpi_2}{\varpi_2}\right). \tag{3}$$

Lemma 3 ([38]): The following Young's inequality is true for $x, y \geq 0$ and $m, n > 1$, such that $\frac{1}{m} + \frac{1}{n} = 1$:

$$xy \leq \frac{x^m}{m} + \frac{y^n}{n}. \tag{4}$$

Lemma 4 ([39]): For the real variables γ_1 and γ_2, and any given constants $u > 0$, $v > 0$, and $\kappa > 0$, the following inequality holds:

$$|\gamma_1|^u|\gamma_2|^v \leq \frac{u}{u+v}\kappa|\gamma_1|^{u+v} + \frac{u}{u+v}\kappa^{\frac{-u}{v}}|\gamma_1|^{u+v}. \tag{5}$$

Furthermore, based on Lemma 4, let $\gamma_1 = 1$, $\gamma_2 = \gamma$, $u = 1-\varsigma$, $v = \varsigma$ and $\kappa = \varsigma^{\frac{\varsigma}{1-\varsigma}}$ for $0 < \varsigma < 1$. Then, equation (5) becomes:

$$|\gamma|^{\varsigma} \leq (1-\varsigma)\varsigma^{\frac{\varsigma}{1-\varsigma}} + |\gamma|. \tag{6}$$

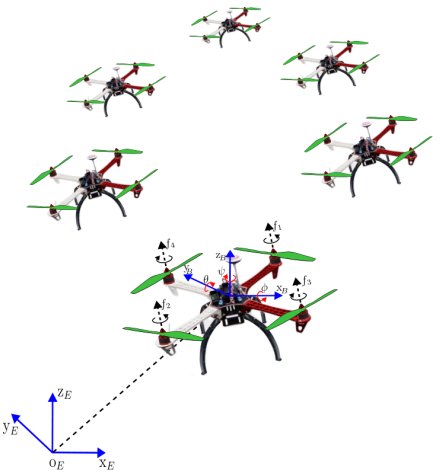

FIGURE 1. Description of the flight formation motion of a multi-QUAV system.

Lemma 5 ([40]): For $\gamma_i \in \mathbb{R}$, $i = 1, \ldots, N$, and $0 < q < 1$, the following inequality holds:

$$\left(\sum_{i=1}^{N}|\gamma_i|\right)^q \leq \sum_{i=1}^{N}|\gamma_i|^q \leq N^{1-q}\left(\sum_{i=1}^{N}|\gamma_i|\right)^q. \tag{7}$$

III. MATHEMATICAL MODEL AND PROBLEM STATEMENT

A. MATHEMATICAL MODEL OF THE MULTI-QUAV SYSTEM

Consider a multi-agent system composed of N quadcopters, as shown in Figure 1, where the quadcopters are assumed to be identical and follow the same mathematical model. The motion of the i-th quadcopter with $i \in \{1, \ldots, N\}$ in space can be decomposed into translational and rotational motion. Each aircraft presents two three-dimensional coordinate frames: one fixed to the earth and one fixed to the i-th body (see Figure 1). Therefore, the complete mathematical model of the i-th quadcopter is described as [11]:

$$\begin{cases} \dot{\xi}_i = \nu_i, \\ m_i\dot{\nu}_i = -m_i g e_z + R_{i,t}u_{i,z}e_z + F_{i,a} + d_{i,\xi}^{\text{ext}}, \\ \dot{\eta}_i = R_{i,r}\,\omega_i, \\ J_i\dot{\omega}_i = -\left(\dot{\omega}_i^T \times J_i\dot{\omega}_i\right) + \tau_{i,m} + \tau_{i,g} + \tau_{i,a} + d_{i,\eta}^{\text{ext}}, \end{cases} \tag{8}$$

where $\xi_i = [x_i, y_i, z_i]^T$, $\nu_i = [u_i, v_i, w_i]^T \in \mathbb{R}^3$, m_i and $g \in \mathbb{R}^+$ represent the position, linear velocity, mass, and acceleration of gravity of the i-th QUAV. The magnitude $u_{i,z} \in \mathbb{R}^+$ denotes the total thrust force generated by the four rotors, while $F_{i,a} = -\text{diag}(\bar{k}_{i,x}, \bar{k}_{i,y}, \bar{k}_{i,z})\dot{\xi}_i \in \mathbb{R}^3$ is the aerodynamic drag force of the same QUAV. In addition, $d_{i,\xi}^{\text{ext}} \in \mathbb{R}^3$ represents the external disturbances in the translational dynamics. On the other hand, $\eta_i = [\phi_i, \theta_i, \psi_i]^T$, $\omega_i = [p_i, q_i, r_i]^T \in \mathbb{R}^3$ and $J_i = \text{diag}(J_{i,x}, J_{i,y}, J_{i,z}) \in \mathbb{R}^{3\times3}$ represent the orientation, angular velocity and moment of inertia of the i-th QUAV. The vector $\tau_{i,m} = [u_{i,\phi}, u_{i,\theta}, u_{i,\psi}]^T \in \mathbb{R}^3$ represents the motor torques, $\tau_{i,g} = -\sum_{\epsilon=1}^{4}(\dot{\eta}_i)^T \times J_{i,r}[0, 0, (-1)^{\epsilon+1}\Omega_{i,\epsilon}]^T \in$

$\mathbb{R}^3$ represents the torques produced by gyroscopic effects, and $\tau_{i,a} = -\text{diag}(\bar{k}_{i,\phi}, \bar{k}_{i,\theta}, \bar{k}_{i,\psi})\eta_i^T \eta_i \in \mathbb{R}^3$ denotes the aerodynamic friction torques. Also, $d_{i,\eta}^{\text{ext}} \in \mathbb{R}^3$ represents the external disturbances in the rotational dynamics, and $e_z = [0, 0, 1]^T \in \mathbb{R}^3$ is a unit vector. Finally, $R_{i,t}$ y $R_{i,r} \in \mathbb{R}^{3\times3}$ represent the rotation matrix and the transformation matrix, respectively, and are defined as [8]:

$$R_{i,t} = \begin{bmatrix} c\psi_i c\theta_i & c\psi_i s\theta_i s\phi_i - s\psi_i c\phi_i & c\psi_i s\theta_i c\phi_i + s\psi_i s\phi_i \\ s\psi_i c\theta_i & s\psi_i s\theta_i s\phi_i + c\psi_i c\phi_i & s\psi_i s\theta_i c\phi_i - c\psi_i s\phi_i \\ -s\theta_i & c\theta_i s\phi_i & c\theta_i c\phi_i \end{bmatrix},$$
$$R_{i,r} = \begin{bmatrix} 1 & s\phi_i\, t\theta_i & c\phi_i\, t\theta_i \\ 0 & c\phi_i & -s\phi_i \\ 0 & s\phi_i / c\theta_i & c\phi_i / c\theta_i \end{bmatrix}, \tag{9}$$

where $s(\bullet)$, $c(\bullet)$, and $t(\bullet)$ are abbreviations of $\sin(\bullet)$, $\cos(\bullet)$, and $\tan(\bullet)$, respectively.

The thrust force $u_{i,z}$ and the motor torques $\tau_{i,m}$ are the control inputs of the QUAV. These control inputs are generated by the aircraft actuators and are calculated as a function of the angular velocities of the four rotors of the aerial vehicle as follows:

$$\begin{bmatrix} u_{i,z} \\ u_{i,\phi} \\ u_{i,\theta} \\ u_{i,\psi} \end{bmatrix} = \begin{bmatrix} \kappa_t & \kappa_t & \kappa_t & \kappa_t \\ -\kappa_t l & \kappa_t l & \kappa_t l & -\kappa_t l \\ \kappa_t l & -\kappa_t l & \kappa_t l & -\kappa_t l \\ -\kappa_d & -\kappa_d & \kappa_d & \kappa_d \end{bmatrix} \begin{bmatrix} \Omega_1 \\ \Omega_2 \\ \Omega_3 \\ \Omega_4 \end{bmatrix}, \tag{10}$$

where $\kappa_t \in \mathbb{R}^+$ is the thrust coefficient, $\kappa_d \in \mathbb{R}^+$ denotes the drag coefficient, and $l \in \mathbb{R}^+$ represents the distance between the centre of mass of the i-th QUAV and the rotors.

Remark 1: In the design of flight controllers for quadcopters, it is common to employ Small Angle Approximation (SAA). This technique approximates the Euler angles (ϕ, θ, ψ) to very small quantities [41], [42]. This approximation is justified because, in practical real-flight situations, the Euler angles of the QUAV tend to vary minimally, and aggressive maneuvers involving large changes in these angles are rarely executed [43], [44].

After performing mathematical operations with the model of the i-th QUAV given in (8) and considering the approximation of the Euler angles in Remark 1, the complete translation and rotation dynamic of the i-th QUAV is expressed as:

$$\begin{cases} \ddot{x}_i = m_i^{-1}\left[(c\phi_i s\theta_i c\psi_i + s\phi_i s\psi_i)u_{i,z} - \bar{k}_{i,x}\dot{x}_i + d_{i,x}^{\text{ext}}\right], \\ \ddot{y}_i = m_i^{-1}\left[(c\phi_i s\theta_i s\psi_i - s\phi_i c\psi_i)u_{i,z} - \bar{k}_{i,y}\dot{y}_i + d_{i,y}^{\text{ext}}\right], \\ \ddot{z}_i = m_i^{-1}\left[(c\phi_i c\theta_i)u_{i,z} - \bar{k}_{i,z}\dot{z}_i + d_{i,z}^{\text{ext}}\right] - g, \\ \ddot{\phi}_i = J_{i,x}^{-1}\left[(J_{i,y} - J_{i,z})\dot{\theta}_i\dot{\psi}_i - J_{i,r}\dot{\theta}_i\overline{\omega}_i - \bar{k}_{i,\phi}\dot{\phi}_i^2 + u_{i,\phi} + d_{i,\phi}^{\text{ext}}\right], \\ \ddot{\theta}_i = J_{i,y}^{-1}\left[(J_{i,z} - J_{i,x})\dot{\phi}_i\dot{\psi}_i + J_{i,r}\dot{\phi}_i\overline{\omega}_i - \bar{k}_{i,\theta}\dot{\theta}_i^2 + u_{i,\theta} + d_{i,\theta}^{\text{ext}}\right], \\ \ddot{\psi}_i = J_{i,z}^{-1}\left[(J_{i,x} - J_{i,y})\dot{\phi}_i\dot{\theta}_i - \bar{k}_{i,\psi}\dot{\psi}_i^2 + u_{i,\psi} + d_{i,\psi}^{\text{ext}}\right], \end{cases} \tag{11}$$

where $\overline{\omega}_i = \Omega_1 - \Omega_2 + \Omega_3 - \Omega_4$ is the total residual speed of the rotor.

Assumption 1: In this research, it is assumed that the drag force $F_{i,a}$, the torques produced by gyroscopic effects $\tau_{i,g}$ and the aerodynamic friction torque $\tau_{i,a}$ constitute the unmodeled internal dynamics of the QUAV. This is because, in practice, it is difficult to identify the aerodynamic coefficients of the aircraft accurately. Therefore, they are considered a type of uncertainty known as **"modeling uncertainty"**, present in both the translational and rotational dynamics of the aircraft:

$$\Delta_{i,\xi}^{\text{m}} = \begin{bmatrix} \Delta_{i,x}^{\text{m}} \\ \Delta_{i,y}^{\text{m}} \\ \Delta_{i,z}^{\text{m}} \end{bmatrix} = F_{i,a} = \begin{bmatrix} -\bar{k}_{i,x}\dot{x}_i \\ -\bar{k}_{i,y}\dot{y}_i \\ -\bar{k}_{i,z}\dot{z}_i \end{bmatrix},$$
$$\Delta_{i,\eta}^{\text{m}} = \begin{bmatrix} \Delta_{i,\phi}^{\text{m}} \\ \Delta_{i,\theta}^{\text{m}} \\ \Delta_{i,\psi}^{\text{m}} \end{bmatrix} = \tau_{i,a} + \tau_{i,g} = \begin{bmatrix} -\bar{k}_{i,\phi}\dot{\phi}_i^2 - J_{i,r}\dot{\theta}_i\overline{\omega}_i \\ -\bar{k}_{i,\theta}\dot{\theta}_i^2 + J_{i,r}\dot{\phi}_i\overline{\omega}_i \\ -\bar{k}_{i,\psi}\dot{\psi}_i^2 \end{bmatrix}. \tag{12}$$

Remark 2: The variation of the QUAV parameters, such as its mass and moments of inertia, also constitutes another type of uncertainty known as **"parametric uncertainty"**. In the translational dynamics, the variation of the mass is expressed as $\Delta_{i,\xi}^{\text{p}} = (m_i + \Delta m_i)$. In the rotational dynamics, the variation of the moments of inertia is expressed as $\Delta_{i,\eta}^{\text{p}} = (J_i + \Delta J_i)$. Both modeling uncertainties and parametric uncertainties are part of the unknown internal uncertainties of the translational dynamics $\Delta_{i,\xi}^{\text{int}} = \Delta_{i,\xi}^{\text{m}} + \Delta_{i,\xi}^{\text{p}}$ and rotational dynamics $\Delta_{i,\eta}^{\text{int}} = \Delta_{i,\eta}^{\text{m}} + \Delta_{i,\eta}^{\text{p}}$ of the QUAV system.

B. PROBLEM STATEMENT

For the design of a formation control system, the dynamic model of translation and rotation of the i-th QUAV, given in (11), can be reformulated in the state space representation as follows:

$$\begin{cases} \dot{x}_{i,1} = x_{i,2}, \\ \dot{x}_{i,2} = m_i^{-1}\left[(cx_{i,7}sx_{i,9}cx_{i,11} + sx_{i,7}sx_{i,11})u_{i,z} + \Delta_{i,x}^{\text{lum}}\right], \\ \dot{x}_{i,3} = x_{i,4}, \\ \dot{x}_{i,4} = m_i^{-1}\left[(cx_{i,7}sx_{i,9}sx_{i,11} - sx_{i,7}cx_{i,11})u_{i,z} + \Delta_{i,y}^{\text{lum}}\right], \\ \dot{x}_{i,5} = x_{i,6}, \\ \dot{x}_{i,6} = m_i^{-1}\left[(cx_{i,7}cx_{i,9})u_{i,z} + \Delta_{i,z}^{\text{lum}}\right] - g, \\ \dot{x}_{i,7} = x_{i,8}, \\ \dot{x}_{i,8} = J_{i,x}^{-1}\left[(J_{i,y} - J_{i,z})\dot{x}_{i,10}\dot{x}_{i,12} + u_{i,\phi} + \Delta_{i,\phi}^{\text{lum}}\right], \\ \dot{x}_{i,9} = x_{i,10}, \\ \dot{x}_{i,10} = J_{i,y}^{-1}\left[(J_{i,z} - J_{i,x})\dot{x}_{i,8}\dot{x}_{i,12} + u_{i,\theta} + \Delta_{i,\theta}^{\text{lum}}\right], \\ \dot{x}_{i,11} = x_{i,12}, \\ \dot{x}_{i,12} = J_{i,z}^{-1}\left[(J_{i,x} - J_{i,y})\dot{x}_{i,8}\dot{x}_{i,10} + u_{i,\psi} + \Delta_{i,\psi}^{\text{lum}}\right], \end{cases} \tag{13}$$

where $x = [x_i, \dot{x}_i, y_i, \dot{y}_i, z_i, \dot{z}_i, \phi_i, \dot{\phi}_i, \theta_i, \dot{\theta}_i, \psi_i, \dot{\psi}_i]^T \in \mathbb{R}^{12}$ is the vector of states.

Remark 3: The terms $\Delta_{i,\kappa}^{\text{lum}}$, where $\kappa = (x, y, z, \phi, \theta, \psi)$ in (13), represent the total lumped uncertainties acting on the translation and rotation dynamics of the QUAV, respectively. These uncertainties include modeling uncertainties, parametric uncertainties, and external disturbances. The total lumped uncertainties are defined as $\Delta_{i,\xi}^{\text{lum}} = \Delta_{i,\xi}^{\text{int}} + d_{i,\xi}^{\text{ext}} = [\Delta_{i,x}^{\text{lum}}, \Delta_{i,y}^{\text{lum}}, \Delta_{i,z}^{\text{lum}}]^T \in \mathbb{R}^3$ and $\Delta_{i,\eta}^{\text{lum}} = \Delta_{i,\eta}^{\text{int}} + d_{i,\eta}^{\text{ext}} =$

$[\Delta_{i,\phi}^{\text{lum}}, \Delta_{i,\theta}^{\text{lum}}, \Delta_{i,\psi}^{\text{lum}}]^T \in \mathbb{R}^3$. It is crucial to note that these total uncertainties are unknown to the formation control system and will not be considered for the control design, which adds an additional challenge.

As is known, QUAV aircraft, in addition to exhibiting nonlinear and strongly coupled dynamics, are considered underactuated mechanical systems with six outputs and four control inputs [9]. To address the underactuation problem, the model given in (13) can be divided into two subsystems: an underactuated position subsystem and a fully actuated attitude subsystem. Therefore, the following two models are introduced and will be used to design the formation control system.

$$\begin{cases} \dot{X}_{i,1}(t) = X_{i,2}(t), \\ \dot{X}_{i,2}(t) = f_{i,\xi}(X_{i,3}, t), \\ \dot{Y}_{i,1}(t) = X_{i,1}(t), \end{cases} \quad \begin{cases} \dot{X}_{i,3}(t) = X_{i,4}(t), \\ \dot{X}_{i,4}(t) = f_{i,\eta}(X_{i,4}, t) + g_{i,\eta}(t)u_{i,\eta}(t), \\ \dot{Y}_{i,2}(t) = X_{i,3}(t). \end{cases} \tag{14}$$

- **Underactuated position subsystem**. Let $X_{i,\xi} = [X_{i,1}, X_{i,2}]^T \in \mathbb{R}^{3\times 2}$ be the vector of states of the underactuated position subsystem, where $X_{i,1} = \xi_i = [\mathrm{x}_{i,1}, \mathrm{x}_{i,3}, \mathrm{x}_{i,5}]$, $X_{i,2} = \nu_i = [\mathrm{x}_{i,2}, \mathrm{x}_{i,4}, \mathrm{x}_{i,6}]$, and $Y_{i,1} = \xi_i$ is the vector of controlled outputs. The function $f_{i,\xi}(X_{i,3}, t) = [f_{i,x}, f_{i,y}, f_{i,z}]^T$ is defined as:

$$f_{i,\xi}(X_{i,3}, t) = \begin{bmatrix} f_{i,x} \\ f_{i,y} \\ f_{i,z} \end{bmatrix} = \begin{bmatrix} m_i^{-1}\left[(c\phi_i s\theta_i c\psi_i + s\phi_i s\psi_i)u_{i,z}\right] \\ m_i^{-1}\left[(c\phi_i s\theta_i s\psi_i - s\phi_i c\psi_i)u_{i,z}\right] \\ m_i^{-1}\left[(c\phi_i c\theta_i)u_{i,z} - g\right] \end{bmatrix}. \tag{15}$$

Remark 4: The vector $f_{i,\xi}(X_{i,3}, t)$ represents the virtual control inputs for the underactuated position subsystem, corresponding to the forces along the x, y and z directions. These expressions are introduced to address the underactuation problem and mitigate the coupling between the translational and rotational dynamics of the QUAV system.

- **Fully actuated attitude subsystem**. Let $X_{i,\eta} = [X_{i,3}, X_{i,4}]^T \in \mathbb{R}^{3\times 2}$ be the state vector of the fully actuated attitude subsystem, where $X_{i,3} = \eta_i = [\mathrm{x}_{i,7}, \mathrm{x}_{i,9}, \mathrm{x}_{i,11}]$, $X_{i,4} = \omega_i = [\mathrm{x}_{i,8}, \mathrm{x}_{i,10}, \mathrm{x}_{i,12}]$, and $u_{i,\eta} = [u_{i,\phi}, u_{i,\theta}, u_{i,\psi}]^T \in \mathbb{R}^3$ is the vector of control inputs. $Y_{i,2} = [\phi_i, \theta_i, \psi_i]^T \in \mathbb{R}^3$ is the vector of controlled outputs. The functions $f_{i,\eta}(X_{i,4}, t)$ y $g_{i,\eta}(t)$ are defined as:

$$f_{i,\eta}(X_{i,2}, t) = \begin{bmatrix} f_{i,\phi} \\ f_{i,\theta} \\ f_{i,\psi} \end{bmatrix} = \begin{bmatrix} J_{i,x}^{-1}\left[(J_{i,y} - J_{i,z})\dot{\theta}_i\dot{\psi}_i\right] \\ J_{i,y}^{-1}\left[(J_{i,z} - J_{i,x})\dot{\phi}_i\dot{\psi}_i\right] \\ J_{i,z}^{-1}\left[(J_{i,x} - J_{i,y})\dot{\phi}_i\dot{\theta}_i\right] \end{bmatrix},$$
$$g_{i,\eta}(t) = \begin{bmatrix} g_{i,\phi} \\ g_{i,\theta} \\ g_{i,\psi} \end{bmatrix} = \begin{bmatrix} J_{i,x}^{-1} \\ J_{i,y}^{-1} \\ J_{i,z}^{-1} \end{bmatrix}. \tag{16}$$

C. CONTROL OBJECTIVE

The main objective of this article is to design a robust formation control strategy for a multi-QUAV system using a leader-follower scheme to achieve high performance and robust flight formation capability in the presence of large lumped uncertainties. To achieve this goal, the formation control system must meet the following requirements:

- Reach the desired formation pattern in a short time and maintain its alignment throughout the flight mission while following the reference Cartesian trajectory.
- The formation tracking errors must converge to zero in a finite time and remain in the vicinity of the origin, i.e.:

$$\begin{cases} \lim_{t\to t_f}(\xi_i - \xi_j) \to (\delta_{ij}), \\ \lim_{t\to t_f}(\xi_i - \xi_0) \to (\delta_{i0}), \end{cases} \tag{17}$$

  where $\delta_{ij}^{\xi} = [\delta_{ij}^x, \delta_{ij}^y, \delta_{ij}^z]^T \in \mathbb{R}^3$ represents the desired position deviation between the i-th aircraft and the j-th aircraft that determines the desired formation pattern.
- The formation control law must ensure robust adaptive capability in large lumped uncertainties, similar to those that a multi-QUAV system would face in a real flight scenario.

IV. FLIGHT FORMATION CONTROLLER DESIGN

A. ROBUST FINITE-TIME DISTRIBUTED CONSENSUS FORMATION CONTROL PROTOCOL (RFDCFCP)

Considering the underactuated position subsystem in (14). We define the consensus formation error for the i-th QUAV as:

$$e_{i,1}^{\xi} = \sum_{j=1}^{N} a_{ij}(\xi_i - \xi_j - \delta_{ij}) + b_i(\xi_i - \xi_0 - \delta_{i0}),$$
$$\dot{e}_{i,1}^{\xi} = \sum_{j=1}^{N} a_{ij}(\nu_i - \nu_j) + b_i(\nu_i - \nu_0), \tag{18}$$

where ξ_i, ν_i and ξ_0, ν_0 denote the position and linear velocity of the i-th follower QUAV and the group leader, respectively. $\delta_{ij}^{\xi} = [\delta_{ij}^x, \delta_{ij}^y, \delta_{ij}^z]^T \in \mathbb{R}^3$ represents the desired position deviation between the i-th aircraft and the j-th aircraft.

Remark 5: The formation errors in (18) can also be expressed compactly for a general multi-agent system as follows:

$$E_{\xi} = (L + B) \otimes I_3 \cdot [\Xi - ([1, \ldots, 1]^T)_{N\times 1} \otimes \xi_0 - \overline{\Delta}]^T,$$
$$E_{\nu} = (L + B) \otimes I_3 \cdot [V - ([1, \ldots, 1]^T)_{N\times 1} \otimes \dot{\xi}_0]^T, \tag{19}$$

where $E_{\xi} = [e_{1,1}^{\xi}, .., e_{N,1}^{\xi}]^T$ and $E_{\nu} = [\dot{e}_{1,1}^{\xi}, .., \dot{e}_{N,1}^{\xi}]^T$ are the consensus formation errors, $\Xi = [\xi_1, \ldots, \xi_N]^T$ and $V = [\nu_1, \nu_2, \ldots, \nu_N]^T$ represent the position and velocity of the QUAV agents. $\overline{\Delta} = [\delta_{0j}, \delta_{1j}, \ldots, \delta_{Nj}]^T$, and $\otimes$ denotes the Kronecker product.

Considering (18), we define the first Control Lyapunov Function (CLF) as:

$$V_{i,1}^{\xi} = \frac{1}{2}(e_{i,1}^{\xi})^2. \tag{20}$$

Deriving in time (20), we obtain:

$$\dot{V}_{i,1}^{\xi} = e_{i,1}^{\xi}\dot{e}_{i,1}^{\xi} = e_{i,1}^{\xi}\Big(\sum_{j=1}^{N} a_{ij}(v_i - v_j) + b_i(v_i - v_0)\Big)$$
$$= e_{i,1}^{\xi}\Big((\sum_{j=1}^{N} a_{ij} + b_i)v_i - \sum_{j=1}^{N} a_{ij}v_j - b_i v_0\Big). \quad (21)$$

To guarantee the stability of the first CLF, i.e. $\dot{V}_{i,1}^{\xi} \leq 0$, we assume v_i as the controlling term. Therefore, we introduce a virtual control input Υ_i^{ξ}, such that $v_i = \Upsilon_i^{\xi}$, and define it as:

$$\Upsilon_i^{\xi} = \frac{1}{\sum_{j=1}^{N} a_{ij} + b_i}\Big(\sum_{j=1}^{N} a_{ij}v_j + b_i v_0 - k_{\xi}e_{i,1}^{\xi}\Big), \quad (22)$$

where $k_{\xi} = \text{diag}(k_x, k_y, k_z) \in \mathbb{R}^{3\times 3}$ is a positive definite diagonal matrix representing the controller parameters, with parameters $k_x > 0, k_y > 0, k_z > 0$.

Considering the virtual control input Υ_i^{ξ}, a new consensus formation error variable defined as:

$$e_{i,2}^{\xi} = v_i - \Upsilon_i^{\xi}$$
$$= v_i - \frac{1}{\sum_{j=1}^{N} a_{ij} + b_i}\Big(\sum_{j=1}^{N} a_{ij}v_j + b_i v_0 - k_{\xi}e_{i,1}^{\xi}\Big). \quad (23)$$

Deriving in time (23) and considering the underactuated position subsystem in (14), we obtain:

$$\dot{e}_{i,2}^{\xi} = \dot{v}_i - \frac{1}{\sum_{j=1}^{N} a_{ij}+b_i}\Big(\sum_{j=1}^{N} a_{ij}\dot{v}_j + b_i\dot{v}_0 - k_{\xi}\dot{e}_1^{\xi}\Big)$$
$$= f_{i,\xi} - \frac{1}{\sum_{j=1}^{N} a_{ij}+b_i}\Big(\sum_{j=1}^{N} a_{ij}\dot{v}_j + b_i\dot{v}_0 - k_{\xi}\dot{e}_1^{\xi}\Big). \quad (24)$$

The introduction of $e_{i,2}^{\xi}$ forces the derivative in time of the first CLF to have the following form:

$$\dot{V}_{i,1}^{\xi} = e_{i,1}^{\xi}\Big((\sum_{j=1}^{N} a_{ij}+b_i)[e_{i,2}^{\xi}+\Upsilon_i^{\xi}] - \sum_{j=1}^{N} a_{ij}v_j - b_i v_0\Big)$$
$$= e_{i,1}^{\xi}\Big((\sum_{j=1}^{N} a_{ij}+b_i)e_{i,2}^{\xi} + \Big(\frac{1}{\sum_{j=1}^{N} a_{ij} + b_i}(\sum_{j=1}^{N} a_{ij}v_j$$
$$+ b_i v_0 - k_{\xi}e_{i,1}^{\xi})(\sum_{j=1}^{N} a_{ij} + b_i) - \sum_{j=1}^{N} a_{ij}v_j - b_i v_0\Big)$$
$$= -k_{\xi}(e_1^{\xi})^2 + (\sum_{j=1}^{N} a_{ij} + b_i)e_{i,1}^{\xi}e_{i,2}^{\xi}. \quad (25)$$

It is clear that if $e_{i2}^{\xi} = 0$, $\dot{V}_1^{\xi} \leq 0$ is guaranteed. The goal now is to achieve that $e_{i,2}^{\xi} = 0$. To address this purpose, in the present stage of the formation control design, we implement a recursive second-order sliding mode structure inspired by the works [45], [46]. To this end, in this research, we propose a novel integral non-singular fast terminal recursive sliding surface, defined by:

$$\sigma_{i,\xi} = e_{i,2}^{\xi} + \int_0^t \Big[\alpha_1^{\xi}e_{i,2}^{\xi} + \beta_1^{\xi}|e_{i,2}^{\xi}|^{\lambda_{\xi}}\text{sign}(e_{i,2}^{\xi})\Big]dt,$$
$$s_{i,\xi} = \sigma_{i,\xi} + \int_0^t \Big[\alpha_2^{\xi}\sigma_{i,\xi} + \beta_2^{\xi}|\sigma_{i,\xi}|^{\lambda_{\xi}}\text{sign}(\sigma_{i,\xi})\Big]dt, \quad (26)$$

where $\alpha_1^{\xi}, \alpha_2^{\xi}, \beta_1^{\xi}, \beta_2^{\xi} \in \mathbb{R}^{3\times 3}$ are positive definite diagonal matrices representing the controller parameters. The exponent λ_{ξ} satisfies $0 < \lambda_{\xi} < 1$. Deriving in time (26), we obtain the following expression:

$$\dot{\sigma}_{i,\xi} = \dot{e}_{i,2}^{\xi} + \alpha_1^{\xi}e_{i,2}^{\xi} + \beta_1^{\xi}|e_{i,2}^{\xi}|^{\lambda_{\xi}}\text{sign}(e_{i,2}^{\xi}),$$
$$\dot{s}_{i,\xi} = \dot{\sigma}_{i,\xi} + \alpha_2^{\xi}\sigma_{i,\xi} + \beta_2^{\xi}|\sigma_{i,\xi}|^{\lambda_{\xi}}\text{sign}(\sigma_{i,\xi}). \quad (27)$$

The robust formation control law required to achieve the desired formation pattern in a finite time and maintain its alignment throughout the flight mission is designed for the i-th QUAV as follows:

$$f_{i,\xi} = \Big[u_{i,\xi}^{\text{eq}} + u_{i,\xi}^{\text{r}}\Big], \quad (28)$$

where $u_{i,\xi}^{\text{r}}$ represents the reaching control term and is responsible for providing fast convergence of the system states from any initial state to the sliding surface $s_{i,\xi}$ by compensating for nonlinearities and uncertainties, while $u_{i,\xi}^{\text{eq}}$ represents the equivalent control term and is responsible for maintaining the system states on the sliding surface $s_{i,\xi} = 0$.

To achieve a fast convergence rate in a finite time to the sliding surface, a reach control term proportional to the power rate is proposed:

$$u_{i,\xi}^{\text{r}} = -\bar{k}_1^{\xi}s_{i,\xi} - \bar{k}_2^{\xi}|s_{i,\xi}|^{\lambda_{\xi}}\text{sign}(s_{i,\xi}), \quad (29)$$

where $\bar{k}_1^{\xi}$ and $\bar{k}_2^{\xi}$ are positive definite diagonal matrices representing the gains of the reaching control term. The exponent λ_{ξ} satisfies $0 < \lambda_{\xi} < 1$.

On the other hand, the equivalent control term $u_{i,\xi}^{\text{eq}}$ can be obtained from the sliding mode recursive structure (26). For this purpose, we define the second CLF as follows:

$$V_{i,2}^{\xi} = \frac{1}{2}(s_{i,\xi})^2. \quad (30)$$

Deriving in time (30) and substituting (27), we obtain:

$$\dot{V}_{i,2}^{\xi} = s_{i,\xi}(\dot{s}_{i,\xi})$$
$$= s_{i,\xi}\Big(\dot{\sigma}_{i,\xi} + \alpha_2^{\xi}\sigma_{i,\xi} + \beta_2^{\xi}|\sigma_{i,\xi}|^{\lambda_{\xi}}\text{sign}(\sigma_{i,\xi})\Big)$$
$$= s_{i,\xi}\Big(\dot{e}_{i,2}^{\xi} + \alpha_1^{\xi}e_{i,2}^{\xi} + \beta_1^{\xi}|e_{i,2}^{\xi}|^{\lambda_{\xi}}\text{sign}(e_{i,2}^{\xi})$$
$$+ \alpha_2^{\xi}\sigma_{i,\xi} + \beta_2^{\xi}|\sigma_{i,\xi}|^{\lambda_{\xi}}\text{sign}(\sigma_{i,\xi})\Big)$$
$$= s_{i,\xi}\Big(f_{i,\xi} - \frac{1}{\sum_{j=1}^{N} a_{ij}+b_i}\Big(\sum_{j=1}^{N} a_{ij}\dot{v}_j + b_i\dot{v}_0 - k_{\xi}\dot{e}_1^{\xi}\Big)$$

$$+\alpha_1^{\xi} e_{i,2}^{\xi} + \beta_1^{\xi} |e_{i,2}^{\xi}|^{\lambda_\xi} \text{sign}(e_{i,2}^{\xi}) + \alpha_2^{\xi} \sigma_{i,\xi} + \beta_2^{\xi} |\sigma_{i,\xi}|^{\lambda_\xi} \text{sign}(\sigma_{i,\xi}) \Big). \quad (31)$$

The stability of the second CLF is guaranteed when the sliding manifold is reached, i.e., $s_{i,\xi} = \dot{s}_{i,\xi} = 0$. Thus, for this in (31), we consider $f_{i,\xi} = u_{i,\xi}^{\text{eq}}$. Therefore, the equivalent control term is designed as follows:

$$\begin{aligned} u_{i,\xi}^{\text{eq}} = & \frac{1}{\sum_{j=1}^{N} a_{ij} + b_i} \Big(\sum_{j=1}^{N} a_{ij} \dot{v}_j + b_i \dot{v}_0 - k_\xi \dot{e}_1^{\xi} \Big) \\ & - \alpha_1^{\xi} e_{i,2}^{\xi} - \beta_1^{\xi} |e_{i,2}^{\xi}|^{\lambda_\xi} \text{sign}(e_{i,2}^{\xi}) - \alpha_2^{\xi} \sigma_{i,\xi} \\ & - \beta_2^{\xi} |\sigma_{i,\xi}|^{\lambda_\xi} \text{sign}(\sigma_{i,\xi}). \end{aligned} \quad (32)$$

Now, the total thrust force $u_{i,z}$ and the desired attitude angles (ϕ_i^d, θ_i^d) are defined as a function of the virtual forces $(f_{i,x}, f_{i,y}, f_{i,z})$, so recalling the expression in (15) and combining with (28), and performing some mathematical operations we obtain the total thrust $u_{i,z}$ and the desired angles for the i-th QUAV as:

$$\begin{cases} u_{i,z} = m_i \sqrt{(f_{i,x})^2 + (f_{i,y})^2 + (f_{i,z} + g)^2}, \\ \phi_i^d = \text{asin}\left[\dfrac{m_i}{u_{i,z}} \left(f_{i,x} \sin\psi_i^d - f_{i,y} \cos\psi_i^d \right) \right], \\ \theta_i^d = \text{atan}\left[\dfrac{1}{f_{i,z} + g} \left(f_{i,x} \cos\psi_i^d + f_{i,y} \sin\psi_i^d \right) \right]. \end{cases} \quad (33)$$

B. ROBUST FINITE-TIME ATTITUDE STABILIZATION CONTROL (RFASC)

Considering the fully actuated attitude subsystem in (14). We define the attitude tracking error for the i-th QUAV as follows:

$$\begin{aligned} e_{i,1}^{\eta} &= \eta_i - \eta_i^d, \\ \dot{e}_{i,1}^{\eta} &= \dot{\eta}_i - \dot{\eta}_i^d, \end{aligned} \quad (34)$$

where $\eta_i = [\phi_i, \theta_i, \psi_i]^T \in \mathbb{R}^3$ and $\eta_i^d = [\phi_i^d, \theta_i^d, \psi_i^d]^T \in \mathbb{R}^3$ represent the Euler orientation angles and the desired attitude signal, respectively.

In this case, the control law that allows tracking the desired attitude angles, generated by the outer loop RFDCFCP, stably and in a finite time for the i-th QUAV, is designed as:

$$u_{i,\eta} = g_{i,\eta}^{-1} \left[u_{i,\eta}^{\text{eq}} + u_{i,\eta}^{\text{r}} \right], \quad (35)$$

where $u_{i,\eta}^{\text{eq}}$ and $u_{i,\eta}^{\text{r}}$ represent the equivalent control term and the reaching control term for the fully actuated attitude subsystem, respectively. Therefore, performing the same procedure as the RFDCFCP, the reach control term $u_{i,\eta}^{\text{r}}$ and the equivalent control term $u_{i,\eta}^{\text{eq}}$ are designed as follows:

$$u_{i,\eta}^{\text{r}} = -\bar{k}_1^{\eta} s_{i,\eta} - \bar{k}_2^{\eta} |s_{i,\eta}|^{\lambda_\eta} \text{sign}(s_{i,\eta}), \quad (36)$$

and

$$\begin{aligned} u_{i,\eta}^{\text{eq}} = & \ddot{\eta}_i^d - k_\eta \dot{e}_{i,1}^{\eta} - \alpha_1^{\eta} e_{i,2}^{\eta} - \beta_1^{\eta} |e_{i,2}^{\eta}|^{\lambda_\eta} \text{sign}(e_{i,2}^{\eta}) \\ & - \alpha_2^{\eta} \sigma_{i,\eta} - \beta_2^{\eta} |\sigma_{i,\eta}|^{\lambda_\eta} \text{sign}(\sigma_{i,\eta}) - f_{i,\eta}, \end{aligned} \quad (37)$$

where the sliding surfaces $\sigma_{i,\eta}$ and $s_{i,\eta}$ are defined as:

$$\begin{aligned} \sigma_{i,\eta} &= e_{i,2}^{\eta} + \int_0^t \left[\alpha_1^{\eta} e_{i,2}^{\eta} + \beta_1^{\eta} |e_{i,2}^{\eta}|^{\lambda_\eta} \text{sign}(e_{i,2}^{\eta}) \right] dt, \\ s_{i,\eta} &= \sigma_{i,\eta} + \int_0^t \left[\alpha_2^{\eta} \sigma_{i,\eta} + \beta_2^{\eta} |\sigma_{i,\eta}|^{\lambda_\eta} \text{sign}(\sigma_{i,\eta}) \right] dt. \end{aligned} \quad (38)$$

Remark 6: In a practical situation of flight formation, QUAVs are subject to large lumped uncertainties, such as wind gusts, variation of aircraft physical parameters (e.g., transport of a suspended load), and unmodeled internal dynamics, as discussed in Remark 3. It is difficult to acquire precise knowledge of these uncertainties and their upper bounds due to their complex nature, which makes them completely unknown to the controller and could affect its performance in a practical situation. Therefore, it is necessary to implement robust adaptive techniques to the control system that can handle large lumped uncertainties during a flight formation mission.

C. ADAPTIVE LAW DESIGN

In this section, the design of a robust adaptive tuning method is presented to adaptively tune the controller gains without knowing the upper bound of the lumped uncertainties, i.e., counteracting the uncertainties by mitigating the chattering effect. For this purpose, the reach control terms of the RFDCFCP and RFASC presented in (29) and (36) are modified as follows:

$$\begin{cases} u_{i,\xi}^{\text{r}} = -\hat{k}_{i,1}^{\xi} s_{i,\xi} - \hat{k}_{i,2}^{\xi} |s_{i,\xi}|^{\lambda_\xi} \text{sign}(s_{i,\xi}), \\ u_{i,\eta}^{\text{r}} = -\hat{k}_{i,1}^{\eta} s_{i,\eta} - \hat{k}_{i,2}^{\eta} |s_{i,\eta}|^{\lambda_\eta} \text{sign}(s_{i,\eta}), \end{cases} \quad (39)$$

where $\hat{k}_{i,1}^{\xi}, \hat{k}_{i,2}^{\xi}, \hat{k}_{i,1}^{\eta}$ and $\hat{k}_{i,2}^{\eta}$ are the adjustable control gains. Then, the adaptive laws for the reach controller are given by:

$$\begin{cases} \dot{\hat{k}}_{i,1}^{\xi} = k_1^{\xi} |s_{i,\xi}|^2; \quad \dot{\hat{k}}_2^{\xi} = k_2^{\xi} |s_{i,\xi}|^{\lambda_\xi + 1}, \\ \dot{\hat{k}}_1^{\eta} = k_1^{\eta} |s_{i,\eta}|^2; \quad \dot{\hat{k}}_2^{\eta} = k_2^{\eta} |s_{i,\eta}|^{\lambda_\xi + 1}, \end{cases} \quad (40)$$

where $k_1^{\xi}, k_2^{\xi}, k_1^{\eta}$ and k_2^{η} are the adaptive gains employed to tune $\hat{k}_{i,1}^{\xi}, \hat{k}_{i,2}^{\xi}, \hat{k}_{i,1}^{\eta}$ and $\hat{k}_{i,2}^{\eta}$ respectively.

Remark 7: With the control laws designed in (28) and (35), together with the adaptive laws developed in (40), an efficient and effective formation control law with finite time stability is obtained; this proposed approach eliminates the need for prior knowledge of the upper bounds of lumped uncertainties. Moreover, this adaptive control approach mitigates the chattering phenomenon.

V. STABILITY ANALYSIS

This section investigates the finite-time stability of the closed-loop control system under the proposed control law. To analyze the stability, we consider the following theorem:

Theorem 1: Considering the dynamic model of the multi-QUAV system described in (11) and under the formation control law design according to (28) and (35), together with the adaptive laws designed in (40), the closed-loop control system is stable in finite time. This

implies that the formation tracking errors converge to zero in finite time and are constantly maintained in a small region around the origin.

Proof 1: The proof of Theorem 1 consists of two steps: **1) Convergence during the reaching phase:** We prove that the reaching time is bounded, i.e., the states of the multi-QUAV system reach the sliding surface from any initial condition in finite time T_r. **2) Convergence during the sliding phase:** After reaching the sliding surface, we prove that all signals within the closed-loop control system are bounded and that the states of the multi-QUAV system converge to the equilibrium point in finite time T_s.

Step 1. In this step, we demonstrate the convergence of the states of the multi-QUAV system to the sliding surface. To achieve this, using the expression of the sliding surface given in (26) and its derivative in the time given in (27) and replacing the expression (24), we obtain:

$$\begin{aligned}\dot{s}_{i,\xi} &= \dot{\sigma}_{i,\xi} + \alpha_2^{\xi}\sigma_{i,\xi} + \beta_2^{\xi}|\sigma_{i,\xi}|^{\lambda_\xi}\operatorname{sign}(\sigma_{i,\xi}) \\ &= \dot{e}_{i,2}^{\xi} + \alpha_1^{\xi}e_{i,2}^{\xi} + \beta_1^{\xi}|e_{i,2}^{\xi}|^{\lambda_\xi}\operatorname{sign}(e_{i,2}^{\xi}) \\ &\quad + \alpha_2^{\xi}\sigma_{i,\xi} + \beta_2^{\xi}|\sigma_{i,\xi}|^{\lambda_\xi}\operatorname{sign}(\sigma_{i,\xi}) \\ &= f_{i,\xi} - \frac{1}{\sum_{j=1}^{N}a_{ij}+b_i}\left(\sum_{j=1}^{N}a_{ij}\dot{v}_j + b_i\dot{v}_0 - k_\xi\dot{e}_1^{\xi}\right) \\ &\quad + \alpha_1^{\xi}e_{i,2}^{\xi} + \beta_1^{\xi}|e_{i,2}^{\xi}|^{\lambda_\xi}\operatorname{sign}(e_{i,2}^{\xi}) + \alpha_2^{\xi}\sigma_{i,\xi} \\ &\quad + \beta_2^{\xi}|\sigma_{i,\xi}|^{\lambda_\xi}\operatorname{sign}(\sigma_{i,\xi}). \end{aligned} \tag{41}$$

Substituting the control law expression (28) into (41), results in the following expression:

$$\begin{aligned}\dot{s}_{i,\xi} &= \frac{1}{\sum_{j=1}^{N}a_{ij}+b_i}\left(\sum_{j=1}^{N}a_{ij}\dot{v}_j + b_i\dot{v}_0 - k_\xi\dot{e}_1^{\xi}\right) - \alpha_1^{\xi}e_{i,2}^{\xi} \\ &\quad - \beta_1^{\xi}|e_{i,2}^{\xi}|^{\lambda_\xi}\operatorname{sign}(e_{i,2}^{\xi}) - \beta_2^{\xi}|\sigma_{i,\xi}|^{\lambda_\xi}\operatorname{sign}(\sigma_{i,\xi}) \\ &\quad - \alpha_2^{\xi}\sigma_{i,\xi} - \frac{1}{\sum_{j=1}^{N}a_{ij}+b_i}\left(\sum_{j=1}^{N}a_{ij}\dot{v}_j + b_i\dot{v}_0 - k_\xi\dot{e}_1^{\xi}\right) \\ &\quad + \alpha_1^{\xi}e_{i,2}^{\xi} + \beta_1^{\xi}|e_{i,2}^{\xi}|^{\lambda_\xi}\operatorname{sign}(e_{i,2}^{\xi}) + \alpha_2^{\xi}\sigma_{i,\xi} \\ &\quad + \beta_2^{\xi}|\sigma_{i,\xi}|^{\lambda_\xi}\operatorname{sign}(\sigma_{i,\xi}) + u_{i,\xi}^{\mathrm{r}}. \end{aligned} \tag{42}$$

By performing some mathematical operations, we obtain:

$$\dot{s}_{i,\xi} = u_{i,\xi}^{\mathrm{r}} = -\bar{k}_1^{\xi}s_{i,\xi} - \bar{k}_2^{\xi}|s_{i,\xi}|^{\lambda_\xi}\operatorname{sign}(s_{i,\xi}). \tag{43}$$

Then, we choose the following candidate Lyapunov function:

$$V_{s_\xi} = \sum_{i=1}^{N}\frac{1}{2}(s_{i,\xi})^2. \tag{44}$$

Deriving in time (44), substituting (43), and performing the corresponding mathematical operations, we obtain the following expression:

$$\begin{aligned}\dot{V}_{s_\xi} &= \sum_{i=1}^{N}s_{i,\xi}(\dot{s}_{i,\xi}) \\ &= \sum_{i=1}^{N}s_{i,\xi}\left(-\bar{k}_1^{\xi}s_{i,\xi} - \bar{k}_2^{\xi}|s_{i,\xi}|^{\lambda_\xi}\operatorname{sign}(s_{i,\xi})\right) \\ &= -\bar{k}_1^{\xi}\sum_{i=1}^{N}s_{i,\xi}^2 - \bar{k}_2^{\xi}\sum_{i=1}^{N}|s_\xi|^{\lambda_\xi+1} \\ &= -2\bar{k}_1^{\xi}\left[\sum_{i=1}^{N}\frac{1}{2}s_{i,\xi}^2\right] - 2^{\frac{\lambda_\xi+1}{2}}\bar{k}_2^{\xi}\left[\sum_{i=1}^{N}\frac{1}{2}s_{i,\xi}^2\right]^{\frac{\lambda_\xi+1}{2}} \\ &\le -2\bar{k}_1^{\xi}\left[\sum_{i=1}^{N}\frac{1}{2}s_{i,\xi}^2\right] - 2^{\Pi}\bar{k}_2^{\xi}\left[\sum_{i=1}^{N}\frac{1}{2}s_{i,\xi}^2\right]^{\Pi} \\ &\le -2\bar{k}_1^{\xi}\left[V_{s_\xi}\right] - 2^{\Pi}\bar{k}_2^{\xi}\left[V_{s_\xi}\right]^{\Pi}, \end{aligned} \tag{45}$$

where $\Pi = \frac{\lambda_\xi+1}{2}$.

Then, according to Lemma 2, it follows that the states of the multi-QUAV system reach the sliding surface $s_{i,\xi} = 0$ in a finite time given by:

$$T_r = \frac{1}{2\bar{k}_1^{\xi}(1-\Pi)}\ln\left[\frac{2\bar{k}_1^{\xi}V_{s_\xi}^{1-\Pi}(0) + 2^{\Pi}\bar{k}_2^{\xi}}{2^{\Pi}\bar{k}_2^{\xi}}\right]. \tag{46}$$

Step 2. In this step, we demonstrate that the consensus formation errors in (18) and (23), the control law designed in (28), and the adaptive laws designed in (40) will not lead the multi-QUAV system to instability and will converge to the equilibrium point in finite time. To achieve this, the following candidate Lyapunov function is defined:

$$\begin{aligned}V_\xi &= \frac{1}{2}\sum_{i=1}^{N}(e_{i,1}^{\xi})^2 + \frac{1}{2}\sum_{i=1}^{N}(e_{i,2}^{\xi})^2 + \frac{1}{2}\sum_{i=1}^{N}(\sigma_{i,\xi})^2 \\ &\quad + \frac{1}{2}\sum_{i=1}^{N}(s_{i,\xi})^2 + \frac{1}{2}\sum_{i=1}^{N}\zeta_1^{\xi}(\tilde{k}_{i,1}^{\xi})^2 + \frac{1}{2}\sum_{i=1}^{N}\zeta_2^{\xi}(\tilde{k}_{i,2}^{\xi})^2, \end{aligned} \tag{47}$$

where $\tilde{k}_{i,1}^{\xi}$ and $\tilde{k}_{i,2}^{\xi}$ are the adaptive estimation errors. Then $\tilde{k}_{i,1}^{\xi} = \hat{k}_{i,1}^{\xi} - \bar{k}_1^{\xi}$, $\tilde{k}_{i,2}^{\xi} = \hat{k}_{i,2}^{\xi} - \bar{k}_2^{\xi}$, and the constants ζ_1^{ξ}, ζ_2^{ξ} are considered greater than zero.

Deriving in time (47), we obtain:

$$\begin{aligned}\dot{V}_\xi &= \sum_{i=1}^{N}e_{i,1}^{\xi}(\dot{e}_{i,1}^{\xi}) + \sum_{i=1}^{N}e_{i,2}^{\xi}(\dot{e}_{i,2}^{\xi}) + \sum_{i=1}^{N}\sigma_{i,\xi}(\dot{\sigma}_{i,\xi}) \\ &\quad + \sum_{i=1}^{N}s_{i,\xi}(\dot{s}_{i,\xi}) + \sum_{i=1}^{N}\zeta_1^{\xi}\tilde{k}_{i,1}^{\xi}(\dot{\tilde{k}}_{i,1}^{\xi}) + \sum_{i=1}^{N}\zeta_2^{\xi}\tilde{k}_{i,2}^{\xi}(\dot{\tilde{k}}_{i,2}^{\xi}). \end{aligned} \tag{48}$$

By replacing the adaptive parameters into (43), substituting the expression of $\dot{s}_{i,\xi}$ into (48), adding and subtracting some terms, we obtain the following:

$$\begin{aligned}\dot{V}_\xi &= \sum_{i=1}^{N}e_{i,1}^{\xi}(\dot{e}_{i,1}^{\xi}) + \sum_{i=1}^{N}e_{i,2}^{\xi}(\dot{e}_{i,2}^{\xi}) + \sum_{i=1}^{N}\sigma_{i,\xi}(\dot{\sigma}_{i,\xi}) \\ &\quad + \sum_{i=1}^{N}s_{i,\xi}\left(-\hat{k}_{i,1}^{\xi}s_{i,\xi} - \hat{k}_{i,2}^{\xi}|s_{i,\xi}|^{\lambda_\xi}\operatorname{sign}(s_{i,\xi})\right) \end{aligned}$$

$$+\sum_{i=1}^{N}\zeta_1^{\xi}\tilde{k}_{i,1}^{\xi}(\dot{\tilde{k}}_{i,1}^{\xi})+\sum_{i=1}^{N}\zeta_2^{\xi}\tilde{k}_{i,2}^{\xi}(\dot{\tilde{k}}_{i,2}^{\xi})$$
$$=\sum_{i=1}^{N}e_{i,1}^{\xi}(\dot{e}_{i,1}^{\xi})+\sum_{i=1}^{N}e_{i,2}^{\xi}(\dot{e}_{i,2}^{\xi})+\sum_{i=1}^{N}\sigma_{i,\xi}(\dot{\sigma}_{i,\xi})$$
$$+\sum_{i=1}^{N}\big(-\hat{k}_{i,1}^{\xi}(s_{i,\xi})^2-\hat{k}_{i,2}^{\xi}|s_{i,\xi}|^{\lambda_\xi+1}\big)+\sum_{i=1}^{N}\zeta_1^{\xi}\tilde{k}_{i,1}^{\xi}(\dot{\hat{k}}_{i,1}^{\xi})$$
$$+\sum_{i=1}^{N}\zeta_2^{\xi}\tilde{k}_{i,2}^{\xi}(\dot{\hat{k}}_{i,2}^{\xi})+\sum_{i=1}^{N}\big(\bar{k}_1^{\xi}(s_{i,\xi})^2-\bar{k}_1^{\xi}(s_{i,\xi})^2$$
$$+\bar{k}_2^{\xi}|s_{i,\xi}|^{\lambda_\xi+1}-\bar{k}_2^{\xi}|s_{i,\xi}|^{\lambda_\xi+1}\big). \tag{49}$$

Substituting the adaptive laws into (49), we obtain:

$$\dot{V}_\xi=\sum_{i=1}^{N}e_{i,1}^{\xi}(\dot{e}_{i,1}^{\xi})+\sum_{i=1}^{N}e_{i,2}^{\xi}(\dot{e}_{i,2}^{\xi})+\sum_{i=1}^{N}\sigma_{i,\xi}(\dot{\sigma}_{i,\xi})$$
$$+\sum_{i=1}^{N}\big(-\tilde{k}_{i,1}^{\xi}(s_{i,\xi})^2-\tilde{k}_{i,2}^{\xi}|s_{i,\xi}|^{\lambda_\xi+1}\big)$$
$$+\sum_{i=1}^{N}\zeta_1^{\xi}\tilde{k}_{i,1}^{\xi}k_1^{\xi}(s_{i,\xi})^2+\sum_{i=1}^{N}\zeta_2^{\xi}\tilde{k}_{i,2}^{\xi}k_2^{\xi}(s_{i,\xi})^{\lambda_\xi+1}$$
$$+\sum_{i=1}^{N}\big(-\bar{k}_1^{\xi}(s_{i,\xi})^2-\bar{k}_2^{\xi}|s_{i,\xi}|^{\lambda_\xi+1}\big). \tag{50}$$

By grouping common terms together, the following expression is obtained:

$$\dot{V}_\xi=\sum_{i=1}^{N}e_{i,1}^{\xi}(\dot{e}_{i,1}^{\xi})+\sum_{i=1}^{N}e_{i,2}^{\xi}(\dot{e}_{i,2}^{\xi})+\sum_{i=1}^{N}\sigma_{i,\xi}(\dot{\sigma}_{i,\xi})$$
$$+\sum_{i=1}^{N}-\big[(s_{i,\xi})^2-\zeta_1^{\xi}k_1^{\xi}(s_{i,\xi})^2\big]\tilde{k}_{i,1}^{\xi}+$$
$$+\sum_{i=1}^{N}-\big[|s_{i,\xi}|^{\lambda_\xi+1}-\zeta_2^{\xi}k_2^{\xi}|s_{i,\xi}|^{\lambda_\xi+1}\big]\tilde{k}_{i,2}^{\xi}$$
$$+\sum_{i=1}^{N}\big(-\bar{k}_1^{\xi}(s_{i,\xi})^2-\bar{k}_2^{\xi}|s_{i,\xi}|^{\lambda_\xi+1}\big). \tag{51}$$

By substituting the expressions of $\dot{e}_{i,1}^{\xi}$, $\dot{e}_{i,2}^{\xi}$, and $\dot{\sigma}_{i,\xi}$ into (51), we get:

$$\dot{V}_\xi=\sum_{i=1}^{N}e_{i,1}^{\xi}(-k_\xi e_{i,1}^{\xi})+\sum_{i=1}^{N}e_{i,2}^{\xi}\big(-\alpha_1^{\xi}e_{i,2}^{\xi}$$
$$-\beta_1^{\xi}|e_{i,2}^{\xi}|^{\lambda_\xi}\operatorname{sign}(e_{i,2}^{\xi})\big)+\sum_{i=1}^{N}\sigma_{i,\xi}\big(-\alpha_2^{\xi}\sigma_{i,\xi}$$
$$-\beta_2^{\xi}|\sigma_{i,\xi}|^{\lambda_\xi}\operatorname{sign}(\sigma_{i,\xi})\big)-\sum_{i=1}^{N}\mu_1\tilde{k}_{i,1}^{\xi}-\sum_{i=1}^{N}\mu_2\tilde{k}_{i,2}^{\xi}$$
$$+\sum_{i=1}^{N}\big(-\bar{k}_1^{\xi}(s_{i,\xi})^2-\bar{k}_2^{\xi}|s_{i,\xi}|^{\lambda_\xi+1}\big)$$
$$=-\sum_{i=1}^{N}k_\xi(e_{i,1}^{\xi})^2+\sum_{i=1}^{N}\big(-\alpha_1^{\xi}(e_{i,2}^{\xi})^2-\beta_1^{\xi}|e_{i,2}^{\xi}|^{\lambda_\xi+1}\big)$$
$$+\sum_{i=1}^{N}\big(-\alpha_2^{\xi}(\sigma_{i,\xi})^2-\beta_2^{\xi}|\sigma_{i,\xi}|^{\lambda_\xi+1}\big)-\sum_{i=1}^{N}\mu_1\tilde{k}_{i,1}^{\xi}$$
$$-\sum_{i=1}^{N}\mu_2\tilde{k}_{i,2}^{\xi}+\sum_{i=1}^{N}\big(-\bar{k}_1^{\xi}(s_{i,\xi})^2-\bar{k}_2^{\xi}|s_{i,\xi}|^{\lambda_\xi+1}\big), \tag{52}$$

where $\mu_1=(s_{i,\xi})^2-\zeta_1^{\xi}k_1^{\xi}(s_{i,\xi})^2$ and $\mu_2=|s_{i,\xi}|^{\lambda_\xi+1}-\zeta_2^{\xi}k_2^{\xi}|s_{i,\xi}|^{\lambda_\xi+1}$. Employing Young's inequality according to Lemma 3, expression (52) can be rewritten as follows:

$$\dot{V}_\xi=-\sum_{i=1}^{N}k_\xi(e_{i,1}^{\xi})^2+\sum_{i=1}^{N}\bigg(-\alpha_1^{\xi}(e_{i,2}^{\xi})^2$$
$$-\beta_1^{\xi}\frac{1^2+(e_{i,2}^{\xi})^{2(\lambda_\xi+1)}}{2}\bigg)+\sum_{i=1}^{N}\bigg(-\alpha_2^{\xi}(\sigma_{i,\xi})^2$$
$$-\beta_2^{\xi}\frac{1^2+(\sigma_{i,\xi})^{2(\lambda_\xi+1)}}{2}\bigg)+\sum_{i=1}^{N}\bigg(-\bar{k}_1^{\xi}(s_{i,\xi})^2$$
$$-\bar{k}_2^{\xi}\frac{1^2+(s_{i,\xi})^{2(\lambda_\xi+1)}}{2}\bigg)-\sum_{i=1}^{N}\mu_1\bigg(\frac{1^2+(\tilde{k}_{i,1}^{\xi})^2}{2}\bigg)$$
$$-\sum_{i=1}^{N}\mu_2\bigg(\frac{1^2+(\tilde{k}_{i,2}^{\xi})^2}{2}\bigg). \tag{53}$$

Performing the mathematical operations and applying the distributive property to the terms where Lemma 3 was used, the resulting expression is:

$$\dot{V}_\xi=-\sum_{i=1}^{N}2k_\xi\frac{(e_{i,1}^{\xi})^2}{2}+\sum_{i=1}^{N}\bigg(-2\alpha_1^{\xi}\frac{(e_{i,2}^{\xi})^2}{2}$$
$$-\frac{\beta_1^{\xi}}{2}-\beta_1^{\xi}\frac{(e_{i,2}^{\xi})^{2(\lambda_\xi+1)}}{2}\bigg)+\sum_{i=1}^{N}\bigg(-2\alpha_2^{\xi}\frac{(\sigma_{i,\xi})^2}{2}$$
$$-\frac{\beta_2^{\xi}}{2}-\beta_2^{\xi}\frac{(\sigma_{i,\xi})^{2(\lambda_\xi+1)}}{2}\bigg)+\sum_{i=1}^{N}\bigg(-2\bar{k}_1^{\xi}\frac{(s_{i,\xi})^2}{2}$$
$$-\frac{\bar{k}_2^{\xi}}{2}-\bar{k}_2^{\xi}\frac{(s_{i,\xi})^{2(\lambda_\xi+1)}}{2}\bigg)-\sum_{i=1}^{N}\bigg(\frac{\mu_1}{2}+\mu_1\frac{(\tilde{k}_{i,1}^{\xi})^2}{2}\bigg)$$
$$-\sum_{i=1}^{N}\bigg(\frac{\mu_2}{2}+\mu_2\frac{(\tilde{k}_{i,2}^{\xi})^2}{2}\bigg). \tag{54}$$

Multiplying and dividing some terms by $2^{\lambda_\xi+1}$ and grouping the constant terms, the following expression is obtained:

$$\dot{V}_\xi=-\sum_{i=1}^{N}2k_\xi\frac{(e_{i,1}^{\xi})^2}{2}+\sum_{i=1}^{N}\bigg(-2\alpha_1^{\xi}\frac{(e_{i,2}^{\xi})^2}{2}$$
$$-\frac{2^{\lambda_\xi+1}\beta_1^{\xi}}{2}\frac{(e_{i,2}^{\xi})^{2(\lambda_\xi+1)}}{2^{\lambda_\xi+1}}\bigg)+\sum_{i=1}^{N}\bigg(-2\alpha_2^{\xi}\frac{(\sigma_{i,\xi})^2}{2}$$

$$- \frac{2^{\lambda_\xi+1}\beta_2^\xi}{2}\frac{(\sigma_{i,\xi})^{2(\lambda_\xi+1)}}{2^{\lambda_\xi+1}}\Big) + \sum_{i=1}^{N}\Big(- 2\bar{k}_1^\xi \frac{(s_{i,\xi})^2}{2} - \frac{2^{\lambda_\xi+1}\bar{k}_2^\xi}{2}\frac{(s_{i,\xi})^{2(\lambda_\xi+1)}}{2^{\lambda_\xi+1}}\Big) - \sum_{i=1}^{N}\Big(\mu_1\frac{(\tilde{k}_{i,1}^\xi)^2}{2}\Big) - \sum_{i=1}^{N}\Big(\mu_2\frac{(\tilde{k}_{i,2}^\xi)^2}{2}\Big) - \frac{\beta_1^\xi}{2} - \frac{\beta_2^\xi}{2} - \frac{\bar{k}_2^\xi}{2} - \frac{\mu_1}{2} - \frac{\mu_2}{2}. \tag{55}$$

Using the change of variable $\Pi = \lambda_\xi + 1$ for a better representation, we obtain:

$$\dot{V}_\xi = -\sum_{i=1}^{N} 2k_\xi \frac{(e_{i,1}^\xi)^2}{2} + \sum_{i=1}^{N}\Big(- 2\alpha_1^\xi \frac{(e_{i,2}^\xi)^2}{2} - 2^{\Pi-1}\beta_1^\xi\Big[\frac{(e_{i,2}^\xi)^2}{2}\Big]^\Pi\Big) + \sum_{i=1}^{N}\Big(- 2\alpha_2^\xi \frac{(\sigma_{i,\xi})^2}{2} - 2^{\Pi-1}\beta_2^\xi\Big[\frac{(\sigma_{i,\xi})^2}{2}\Big]^\Pi\Big) + \sum_{i=1}^{N}\Big(- 2\bar{k}_1^\xi \frac{(s_{i,\xi})^2}{2} - 2^{\Pi-1}\bar{k}_2^\xi\Big[\frac{(s_{i,\xi})^2}{2}\Big]^\Pi\Big) - \sum_{i=1}^{N}\Big(\mu_1\frac{(\tilde{k}_{i,1}^\xi)^2}{2}\Big) - \sum_{i=1}^{N}\Big(\mu_2\frac{(\tilde{k}_{i,2}^\xi)^2}{2}\Big) - \frac{\beta_1^\xi}{2} - \frac{\beta_2^\xi}{2} - \frac{\bar{k}_2^\xi}{2} - \frac{\mu_1}{2} - \frac{\mu_2}{2}. \tag{56}$$

Applying Lemma 4 to certain terms, the following expression is obtained

$$\dot{V}_\xi = -\sum_{i=1}^{N} 2k_\xi\Big\{\Big[\frac{(e_{i,1}^\xi)^2}{2}\Big]^\Pi - \Xi\Big\} - \sum_{i=1}^{N}\Big(2\alpha_1^\xi\Big\{\Big[\frac{(e_{i,2}^\xi)^2}{2}\Big]^\Pi - \Xi\Big\} - 2^{\Pi-1}\beta_1^\xi\Big[\frac{(e_{i,2}^\xi)^2}{2}\Big]^\Pi\Big) - \sum_{i=1}^{N}\Big(2\alpha_2^\xi\Big\{\Big[\frac{(\sigma_{i,\xi})^2}{2}\Big]^\Pi - \Xi\Big\} - 2^{\Pi-1}\beta_2^\xi\Big[\frac{(\sigma_{i,\xi})^2}{2}\Big]^\Pi\Big) - \sum_{i=1}^{N}\Big(2\bar{k}_1^\xi\Big\{\Big[\frac{(s_{i,\xi})^2}{2}\Big]^\Pi - \Xi\Big\} - 2^{\Pi-1}\bar{k}_2^\xi\Big[\frac{(s_{i,\xi})^2}{2}\Big]^\Pi\Big) - \sum_{i=1}^{N}\mu_1\Big\{\Big[\frac{(\tilde{k}_{i,1}^\xi)^2}{2}\Big]^\Pi - \Xi\Big\} - \sum_{i=1}^{N}\mu_2\Big\{\Big[\frac{(\tilde{k}_{i,2}^\xi)^2}{2}\Big]^\Pi - \Xi\Big\} - \frac{\beta_1^\xi}{2} - \frac{\beta_2^\xi}{2} - \frac{\bar{k}_2^\xi}{2} - \frac{\mu_1}{2} - \frac{\mu_2}{2}, \tag{57}$$

where $\Xi = (1-\Pi)\Pi^{\frac{\Pi}{1-\Pi}}$. Then, applying Lemma 5 and performing some mathematical operations, the expression (57) can be rewritten as:

$$\dot{V}_\xi \leq -\{2k_\xi\}\Big[\sum_{i=1}^{N}\frac{(e_{i,1}^\xi)^2}{2}\Big]^\Pi - \{2\alpha_1^\xi + 2^{\Pi-1}\beta_1^\xi\}\Big[\sum_{i=1}^{N}\frac{(e_{i,2}^\xi)^2}{2}\Big]^\Pi - \{2\alpha_2^\xi + 2^{\Pi-1}\beta_2^\xi\}\Big[\sum_{i=1}^{N}\frac{(\sigma_{i,\xi})^2}{2}\Big]^\Pi - \{2\bar{k}_1^\xi + 2^{\Pi-1}\bar{k}_2^\xi\}\Big[\sum_{i=1}^{N}\frac{(s_{i,\xi})^2}{2}\Big]^\Pi - \{\mu_1\}\Big[\sum_{i=1}^{N}\frac{(\tilde{k}_{i,1}^\xi)^2}{2}\Big]^\Pi - \{\mu_2\}\Big[\sum_{i=1}^{N}\frac{(\tilde{k}_{i,2}^\xi)^2}{2}\Big]^\Pi + \Big\{2k_\xi\Xi + 2\alpha_1^\xi\Xi + 2\alpha_2^\xi\Xi + 2\bar{k}_1^\xi\Xi + \mu_1\Xi + \mu_2\Xi - \frac{\beta_1^\xi}{2} - \frac{\beta_2^\xi}{2} - \frac{\bar{k}_2^\xi}{2} - \frac{\mu_1}{2} - \frac{\mu_2}{2}\Big\} \leq -L_V V^\Pi + F_V, \tag{58}$$

where $L_V = \max\{2k_\xi, 2\alpha_1^\xi + 2^{\Pi-1}\beta_1^\xi, 2\alpha_2^\xi + 2^{\Pi-1}\beta_2^\xi, 2k_1^\xi + 2^{\Pi-1}\bar{k}_2^\xi, \mu_1, \mu_2\}$. $F_V = \max\{2k_{i,\xi}\Xi + 2\alpha_{i,1}^\xi\Xi + 2\alpha_{i,2}^\xi\Xi + 2\bar{k}_1^\xi\Xi + \mu_1\Xi + \mu_2\Xi - \frac{\beta_{i,1}^\xi}{2} - \frac{\beta_{i,2}^\xi}{2} - \frac{\bar{k}_2^\xi}{2} - \frac{\mu_1}{2} - \frac{\mu_2}{2}\}$.

This analysis shows that the Lyapunov candidate function defined in (47) gradually decreases, implying that $V_\xi \leq 0$. As a result, V_ξ is bounded, ensuring all signals within the system are bounded and do not diverge to infinity. Therefore, according to Lemma 1, the states of the multi-QUAV system converge to the equilibrium point in a finite time, defined as:

$$T_s = \frac{1}{(1-\Pi)\varrho L_V}\Big(V^{1-\Pi}(x(0)) - \Big(\frac{F_V}{(1-\varrho)L_V}\Big)^{\frac{1-\Pi}{\Pi}}\Big). \tag{59}$$

Finally, the total time required for the closed-loop control system to reach the desired stability in finite time and for the consensus formation errors $(e_{i,1}^\xi, e_{i,2}^\xi)$ of the RFDCFCP to stabilize at zero equilibrium during the sliding motion $(s_{i,\xi} = 0)$ is given by $T_F^\xi = T_r + T_s$. Thus, completing the proof.

Remark 8: Following the same procedure used in the proof of Theorem 1, it can be shown that the attitude tracking errors $(e_{i,1}^\eta, e_{i,2}^\eta)$ of RFASC stabilize at zero equilibrium during sliding motion $(s_{i,\eta} = 0)$ at finite time T_F^η.

VI. RESULT AND DISCUSSION

To validate the theoretical findings and demonstrate the effectiveness of the proposed control system for flight formation of a multi-QUAV system, the control approach was implemented in the Matlab/Simulink environment under different flight scenarios. For this purpose, we configured two complex and challenging flight scenarios with large uncertainties, similar to real flight conditions QUAVs would encounter. In addition, to evaluate the convergence time, tracking accuracy, and robustness properties of the proposed control method, we conducted a comparative analysis with two recent multi-QUAV formation control approaches: Distributed Robust Formation Control (DRFC) [34] y Predictor-based Constrained Fixed-time Sliding Mode Control (PCFSMC) [35].

The flight formation consists of a virtual leader and three follower QUAVs. The virtual leader is responsible for providing the reference Cartesian trajectory for the multi-QUAV system. The communication topology between the agents is described by a directed graph, where the desired formation pattern is set as an equilateral triangle, as shown in Figure 2. For this purpose, the adjacency matrix, the degree

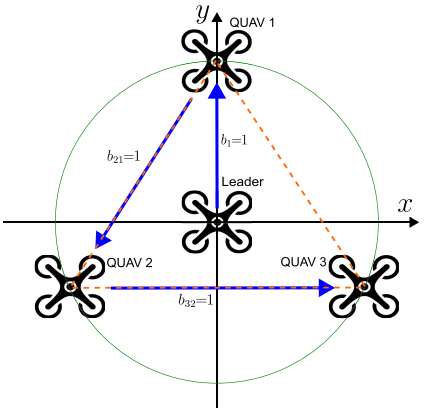

FIGURE 2. Communication topology between QUAV agents and the desired formation pattern.

matrix, and the palace matrix are defined as:

$$A = \begin{bmatrix} 0 & 0 & 0 \\ 1 & 0 & 0 \\ 0 & 1 & 0 \end{bmatrix}, D = \begin{bmatrix} 0 & 0 & 0 \\ 0 & 1 & 0 \\ 0 & 0 & 1 \end{bmatrix}, L = \begin{bmatrix} 0 & 0 & 0 \\ -1 & 1 & 0 \\ 0 & -1 & 1 \end{bmatrix}. \tag{60}$$

The desired position deviation between the leader and the followers is set as follows:

$$\begin{aligned} \delta_{10}^{\xi} &= \delta_1^{\xi} - \delta_0^{\xi}, \\ &= ([0, \sqrt{3}, 0]^T - [0, 0, 0]^T), \\ \delta_{20}^{\xi} &= \delta_2^{\xi} - \delta_0^{\xi}, \\ &= ([\sqrt{3}\cos\left(\frac{5\pi}{6}\right), \sqrt{3}\sin\left(\frac{-\pi}{6}\right), 0]^T - [0, 0, 0]^T), \\ \delta_{30}^{\xi} &= \delta_3^{\xi} - \delta_0^{\xi}, \\ &= ([\sqrt{3}\cos\left(\frac{-\pi}{6}\right), \sqrt{3}\sin\left(\frac{-\pi}{6}\right), 0]^T - [0, 0, 0]^T). \end{aligned} \tag{61}$$

The Adjacency Distance (AD) between the follower QUAVs is set to 3 meters, and the Relative Distance (RD) between the followers and the virtual leader is set to 1.73 meters. This ensures that the desired formation pattern has the geometric shape of an equilateral triangle with 3-meter sides.

The simulations were performed using the DJI-F450 quadcopter model, whose physical parameters are detailed in Table 1. The parameters of the formation control are presented below:

- **RFDCFCP. i) Equivalent control:** $k_x = k_y = k_z = 1.5, \alpha_1^x = \alpha_1^y = \alpha_1^z = 0.0025, \beta_1^x = \beta_1^y = \beta_1^z = 0.0013, \alpha_2^x = \alpha_2^y = \alpha_2^z = 1.2, \beta_2^x = \beta_2^y = \beta_2^z = 4, \lambda_x = \lambda_y = \lambda_z = 0.2$. **ii) Reach control:** $k_1^x = k_1^y = k_1^z = 2, k_2^x = k_2^y = k_2^z = 1.67, \lambda_x = \lambda_y = \lambda_z = 0.2$
- **RFASC: i) Equivalent control:** $k_\phi = k_\theta = 60, k_\psi = 5, \alpha_1^\phi = \alpha_1^\theta = \alpha_1^\psi = 0.176, \beta_1^\phi = \beta_1^\theta = \beta_1^\psi = 0.001, \alpha_2^\phi = \alpha_2^\theta = \alpha_2^\psi = 4.4, \beta_2^\phi = \beta_2^\theta = \beta_2^\psi = 2, \lambda_\phi = \lambda_\theta = \lambda_\psi = 0.2$. *ii)Reachcontrol* : $k_1^\phi = k_1^\theta = k_1^\psi = 2, k_2^\phi = k_2^\theta = k_2^\psi = 1.67, \lambda_\phi = \lambda_\theta = \lambda_\psi = 0.2$

TABLE 1. Physical parameters of the DJI-F450 quadcopter [12].

Parameter	Value	Unit
m_i	1.636	kg
$J_{i,x}$	0.0232	kg m^2
$J_{i,y}$	0.0249	kg m^2
$J_{i,z}$	0.0342	kg m^2
l	0.225	m
g	9.81	m/s^2

A. FLIGHT SCENARIO 1

In this scenario, different uncertainties such as wind gusts, modeling uncertainties, and parametric uncertainties are considered; these lumped uncertainties acting on QUAVs are divided as external disturbances and internal uncertainties, which are defined as:

a) External disturbances: External disturbances affecting the quadcopter dynamics are represented as wind gusts injected into the multi-QUAV system at instant $t = 15$s. The expressions of these external disturbances are given as follows [47]:

$$\begin{cases} d_{i,x}^{\text{ext}} = -1.6\sin(0.1t) + 0.8\sin(0.44t) + 0.16\sin(1.75t) + \\ 0.112\sin(0.28t)\ \text{m/s}^2, \\ d_{i,y}^{\text{ext}} = \sin(0.4t) + \cos(0.7t)\ \text{m/s}^2, \\ d_{i,z}^{\text{ext}} = 0.8\cos(0.7t)\ \text{m/s}^2, \\ d_{i,\phi}^{\text{ext}} = d_{i,\theta}^{\text{ext}} = d_{i,\psi}^{\text{ext}} = 0.02\cos(0.7t)\ \text{rad/s}^2. \end{cases} \tag{62}$$

b) Internal uncertainties: b1) Modeling uncertainties: Represents the unmodeled dynamics of the QUAV, as discussed in Assumption 1. **b2) Parametric uncertainties**: Represents the variation of the physical parameters of the QUAV; for this, we consider parametric uncertainties of +20% on the mass and moments of inertia, i.e. $m_i = 1.963$kg, $J_{i,x} = 0.027$kg m^2, $J_{i,y} = 0.029$kg m^2, $J_{i,z} = 0.041$kg m^2.

For this scenario, the initial positional conditions of the three QUAVs are set as $\xi_1(0) = [-1, 3, 0.01]^T$m, $\xi_2(0) = [-1, -1, 0.01]^T$m, $\xi_3(0) = [1, -3, 0.01]^T$m. The initial velocities of the three aircraft are configured to zero. The following Cartesian trajectory is established for the virtual leader:

$$\xi_0 = [x_0, y_0, z_0]^T = [2.5\cos(0.2t), 2.5\sin(0.2t,), 3]^T\text{m.}, \tag{63}$$

while the yaw angle of each aircraft for this and the other scenarios should be stabilized to zero, i.e., $\psi_i^d = 0$ rad.

The results for this scenario are presented in Figures 3-6. The temporal position response of the three QUAVs is shown in Figure 3. In this figure, the proposed RFDCFCP approach allows the aircraft to reach the desired formation quickly.

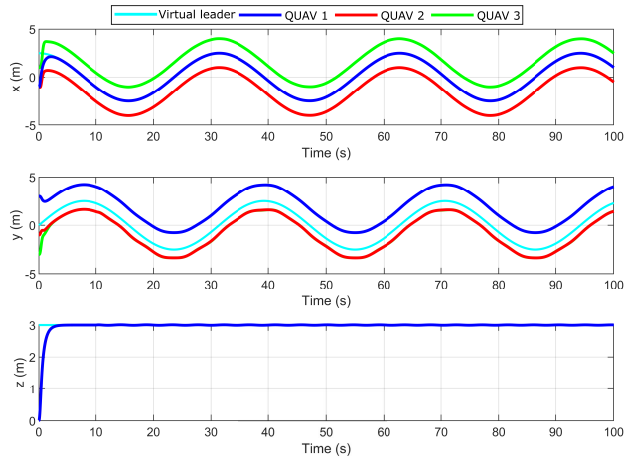

FIGURE 3. Temporal position response of the quadcopters, including the virtual leader.

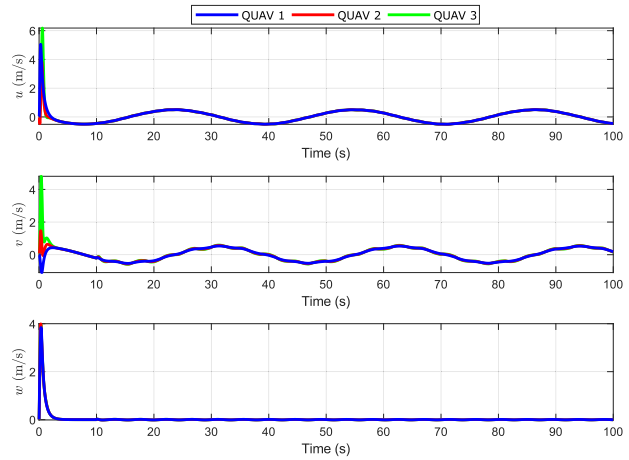

FIGURE 4. Linear velocity of the quadcopters.

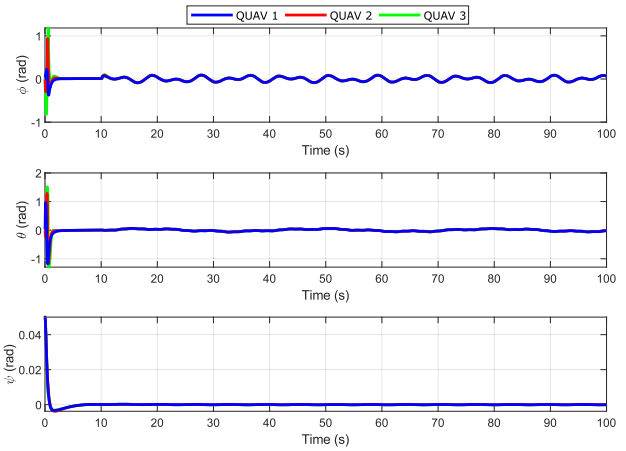

FIGURE 5. Temporal attitude response of the quadcopters.

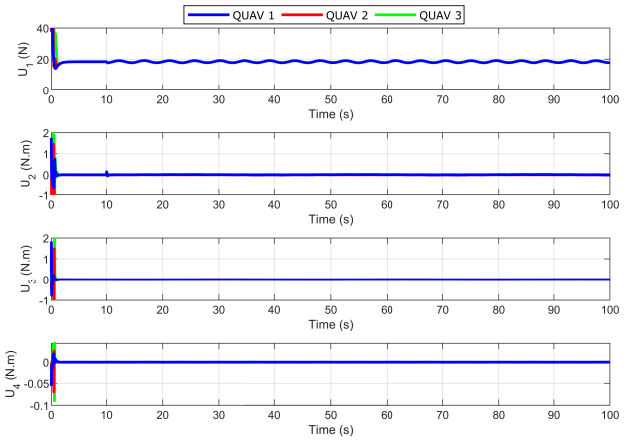

FIGURE 6. Control inputs.

Moreover, the formation has been successfully maintained while following the reference Cartesian trajectory despite large lumped uncertainties. The linear velocity is illustrated in Figure 4, where it can be seen that all three aircraft achieve a fast and stable consensus to maintain the desired formation. The temporal attitude response of the QUAVs is presented in Figure 5, where it is noted that the proposed RFASC approach allows tracking the attitude angles stably, adjusting to the desired attitude generated by the RFDCFCP. The four control inputs of the three QUAVs are illustrated in Figure 6.

For a more comprehensive evaluation, we compared our formation control system with the DRFC [34] and PCFSMC [35] control methods. The results of the three control methods are presented in Figures 7-12. Figure 7 shows the flight formation of the three QUAVs in 3D and 2D under the proposed control system. Our control method succeeds in achieving and maintaining the desired formation pattern stably throughout the flight mission, with accurate tracking of the reference Cartesian trajectory. Although the PCFSMC and DRFC formation controllers in Figures 8 and 9 also succeed in maintaining the desired formation pattern, our proposed method exhibits better tracking accuracy than the other controllers. This is clearly evidenced in the 2D flight formation in Figures 7(b), 8(b), and 9(b), where with our proposed method, all three QUAVs robustly track the reference Cartesian trajectory. Moreover, lumped uncertainties affect our proposed method significantly less, demonstrating its superiority in robustness and adaptability.

On the other hand, the formation tracking errors, adjacent distances, and relative distances for this flight scenario under the three formation controllers are presented in Figures 10, 11, and 12, respectively. The formation tracking errors of the proposed control system in Figure 10(a) achieve fast convergence to zero in finite time and are consistently maintained in the neighborhood of the origin, even in the presence of large lumped uncertainties. Furthermore, the adjacent distances and relative distances presented in Figure 10(b) demonstrate that the desired formation pattern has been successfully maintained without any geometric deformation. The indices converge rapidly to their desired values of 3 meters and 1.73 meters, respectively, and remain constant throughout the flight formation. Compared to the PCFSMC and DRFC

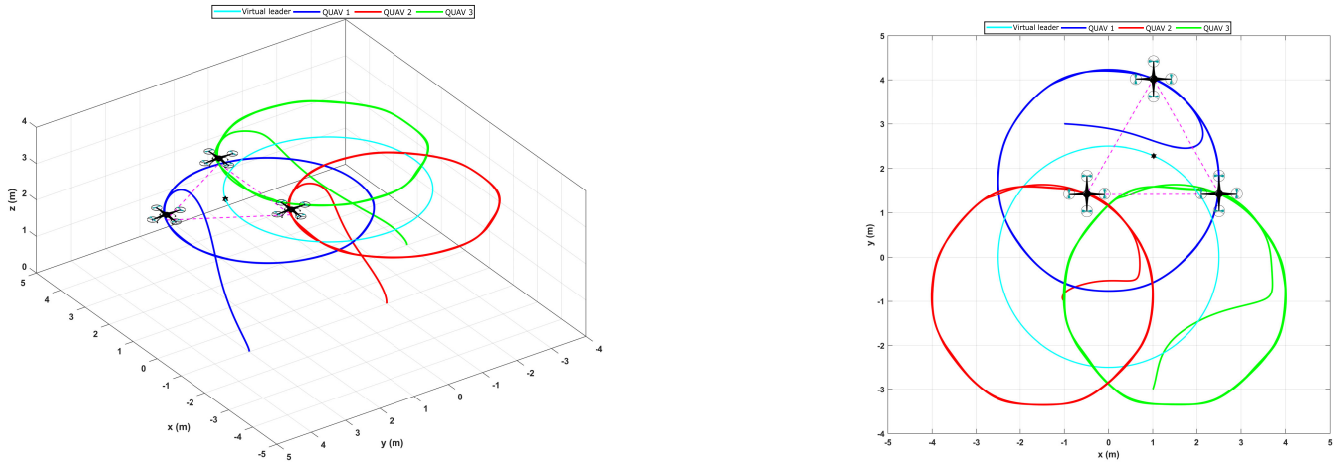

(a) (b)

FIGURE 7. Results of the formation control of the proposed method (a) Viewed in 3D (b) Viewed in 2D.

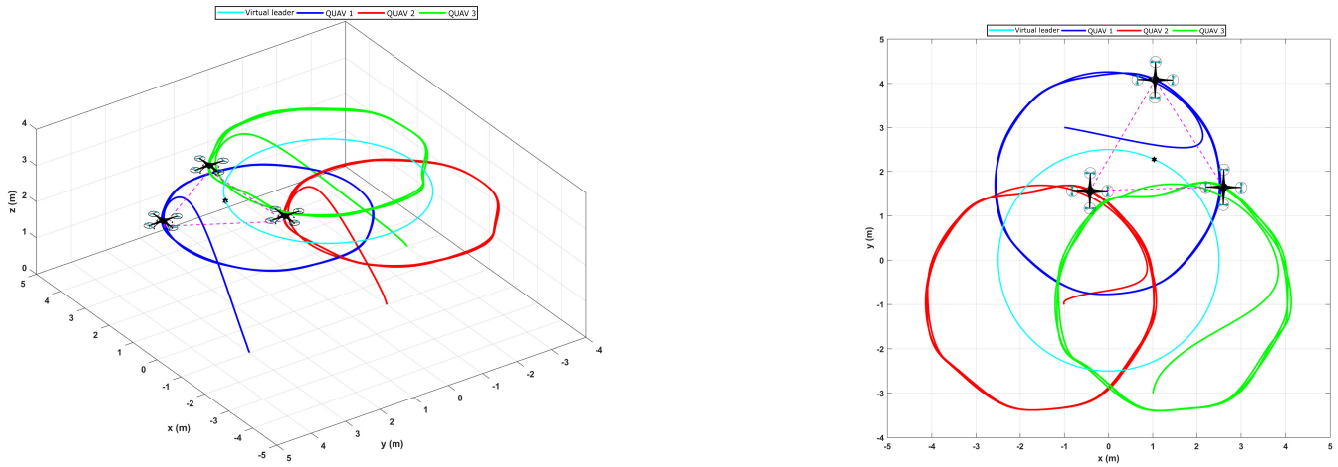

(a) (b)

FIGURE 8. Results of the formation control of the PCFSMC method (a) Viewed in 3D (b) Viewed in 2D.

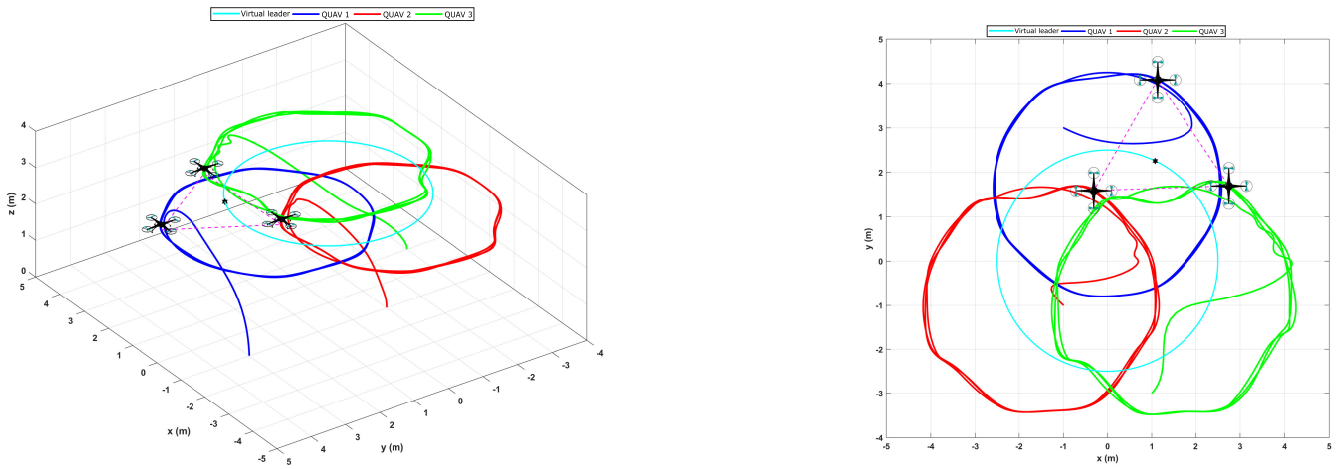

(a) (b)

FIGURE 9. Results of the formation control of the DRFC method (a) Viewed in 3D (b) Viewed in 2D.

control methods shown in Figures 11 and 12, the formation errors also converge to zero. However, by reviewing and comparing the zoomed regions in the interval [30-70]s, as well as the adjacent and relative distances, it can be clearly seen that our control system demonstrates superior robustness and tracking accuracy compared to the PCFSMC and DRFC

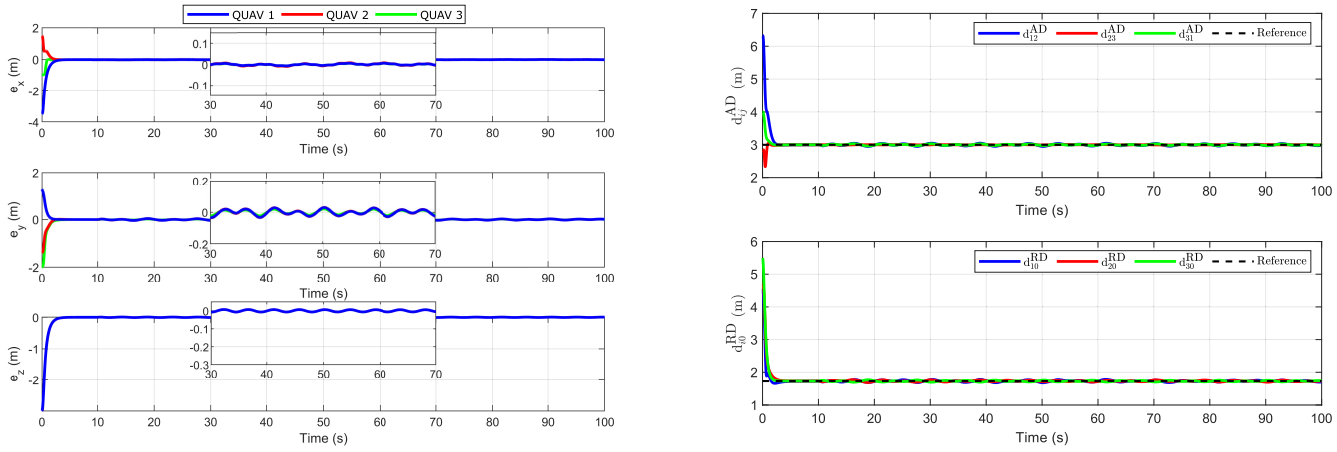

FIGURE 10. Results of the proposed method: (a) Formation errors (b) Adjacent and relative distances.

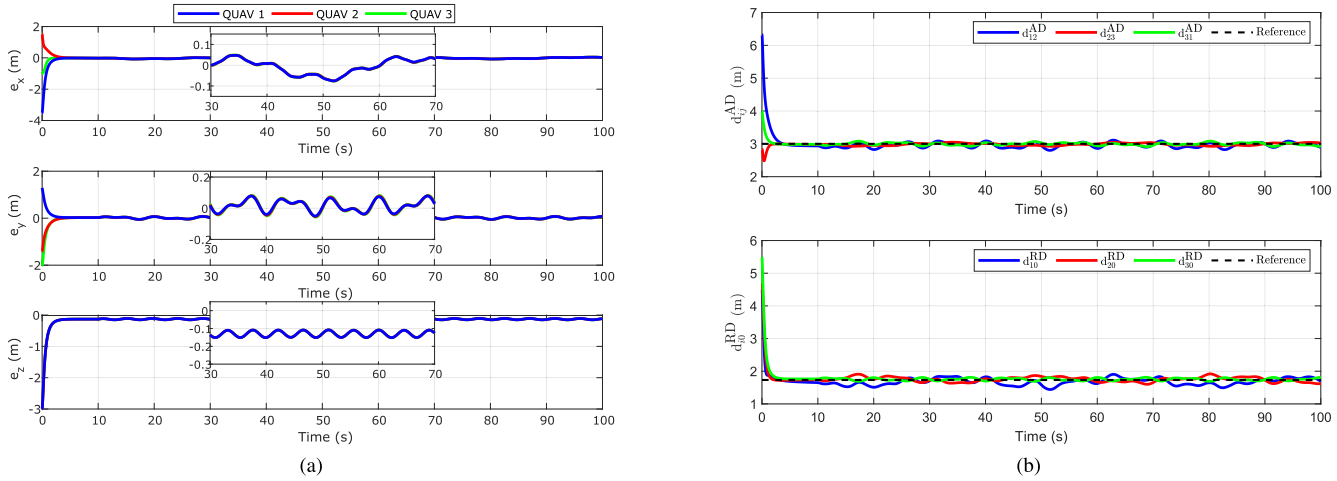

FIGURE 11. Results of the PCFSMC method: (a) Formation errors (b) Adjacent and relative distances.

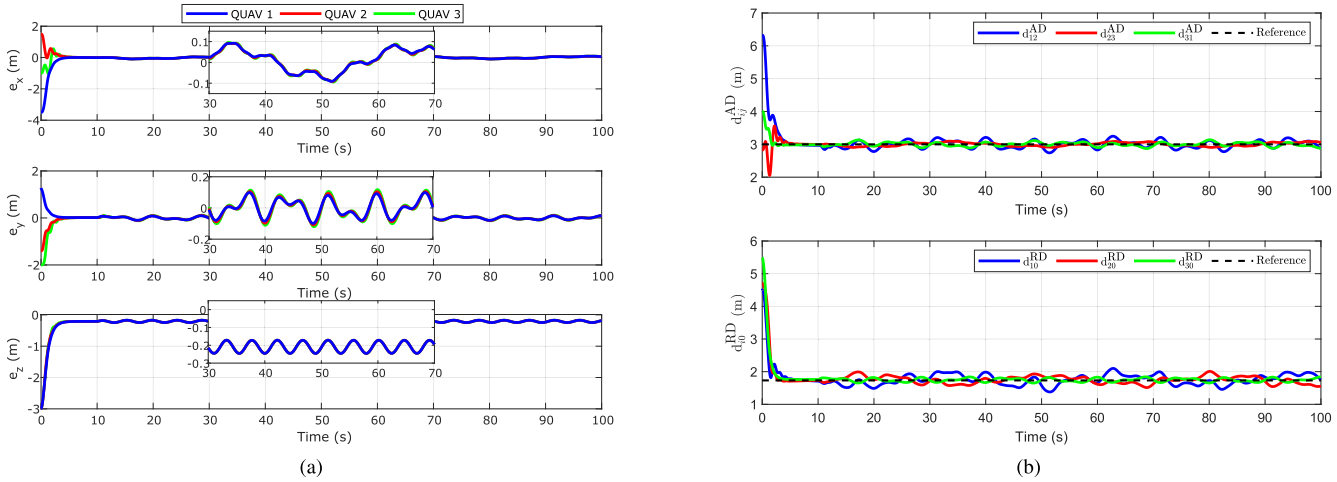

FIGURE 12. Results of the DRFC method: (a) Formation errors (b) Adjacent and relative distances.

methods. Furthermore, it is observed that due to variations in the physical parameters of the aircraft, such as mass and moments of inertia, the altitude formation errors of the PCFSMC and DRFC control methods never reach zero origin. In contrast, our proposed control method maintains these errors at the zero origin throughout the flight mission. This is clearly illustrated in the zoomed regions of Figures 10(a), 11(a), and 12(a), respectively.

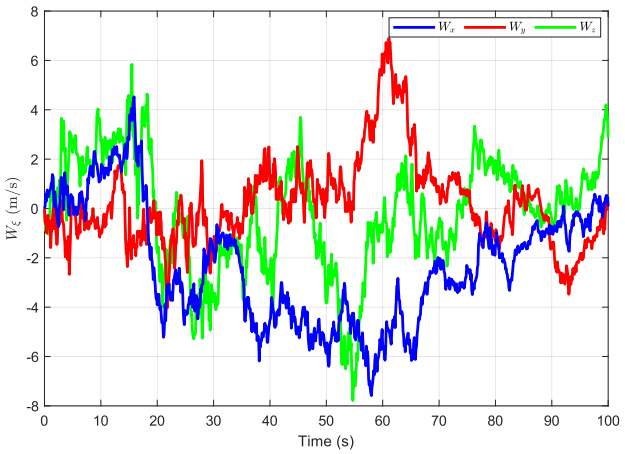

FIGURE 13. Wind speed generated by the Dryden model.

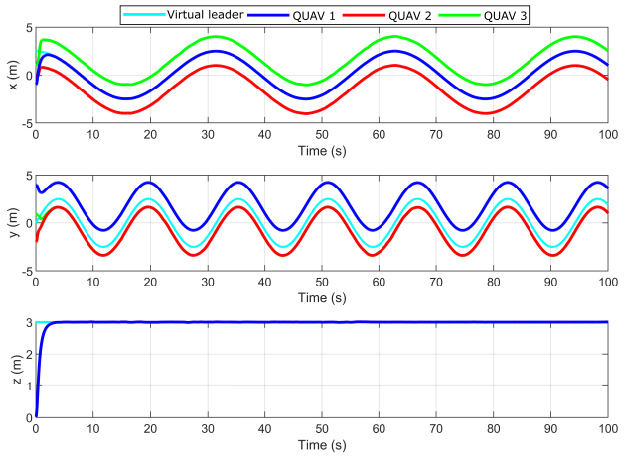

FIGURE 14. Temporal position response of the quadcopters, including the virtual leader.

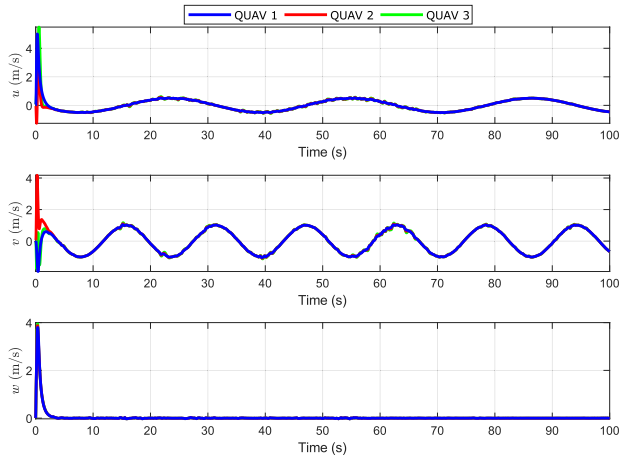

FIGURE 15. Linear velocity of the quadcopters.

To provide a more accurate quantitative comparison of the obtained results and confirm the theoretical findings of the proposed control system, we use the performance indices of

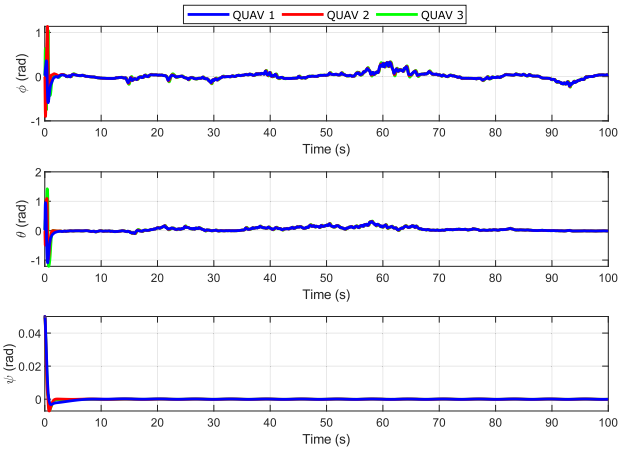

FIGURE 16. Temporal attitude response of the quadcopters.

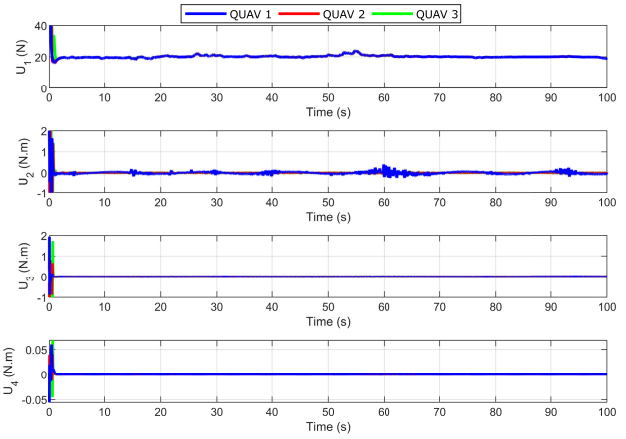

FIGURE 17. Control inputs.

TABLE 2. Convergence time analysis.

Aircraft	Control method	Performance index: Settling time		
		$e^x_{i,1}$	$e^y_{i,1}$	$e^z_{i,1}$
QUAV 1	DRFC	4.298	3.888	-
	PCFSMC	3.801	3.485	-
	Proposed	3.310	1.920	3.140
QUAV 2	DRFC	3.982	3.701	-
	PCFSMC	3.769	3.084	-
	Proposed	2.250	2.090	3.140
QUAV 3	DRFC	4.663	3.330	-
	PCFSMC	1.715	2.884	-
	Proposed	0.920	2.610	3.100

settling time and RMSE. The settling time is defined as the time it takes for the system tracking errors to converge and stabilize within a range of 2.5% concerning the origin. On the other hand, RMSE is a metric that evaluates the performance of the control system in terms of tracking accuracy and robustness. These indices are calculated for each control system and are presented in Tables 2 and 3, respectively.

Table 2 shows that our proposed control system exhibits lower convergence times for all errors than the PCFSMC and

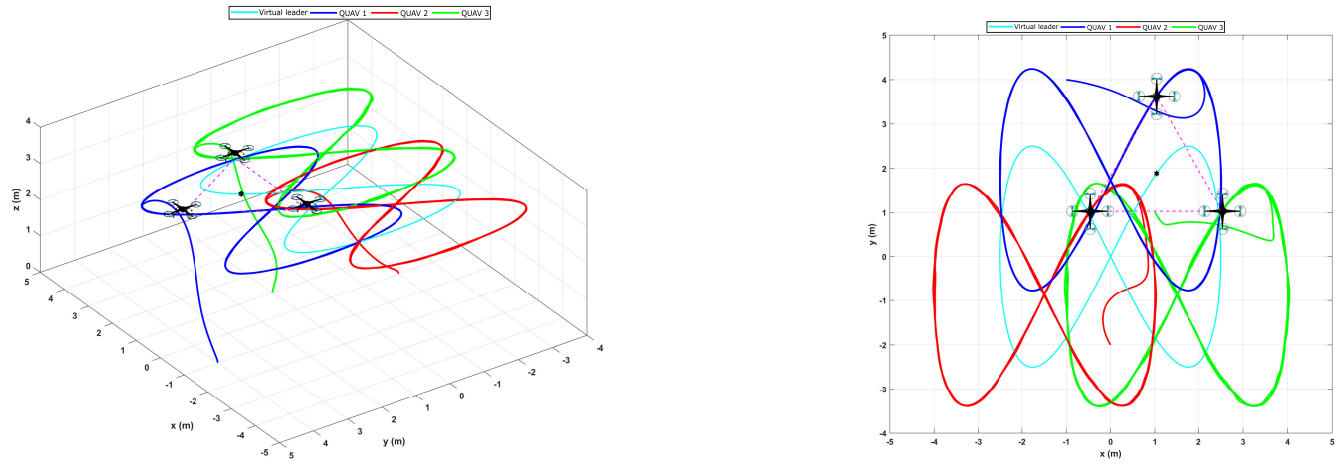

FIGURE 18. Results of the formation control of the proposed method (a) Viewed in 3D (b) Viewed in 2D.

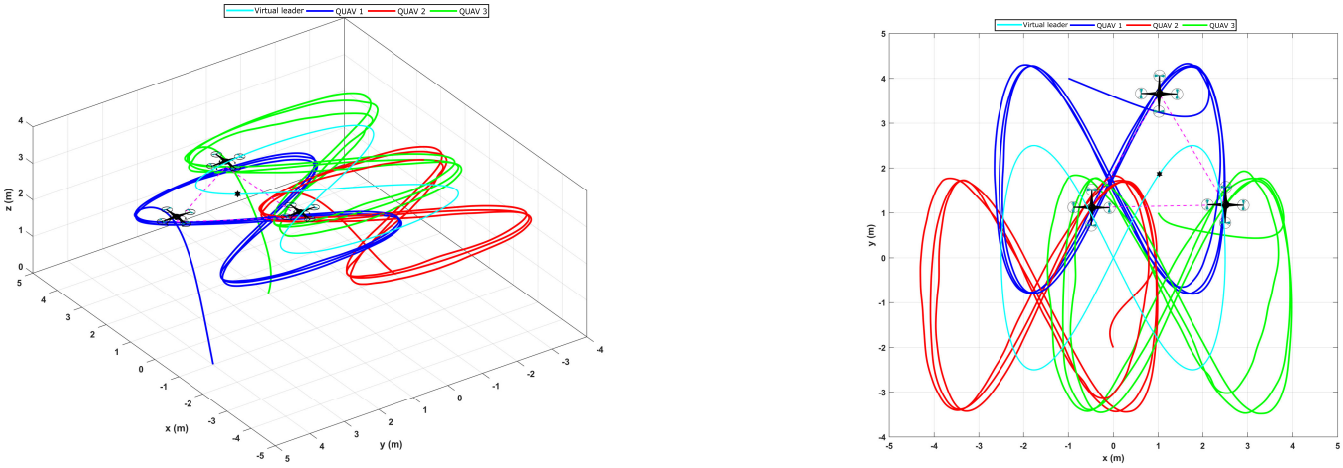

FIGURE 19. Results of the formation control of the PCFSMC method (a) Viewed in 3D (b) Viewed in 2D.

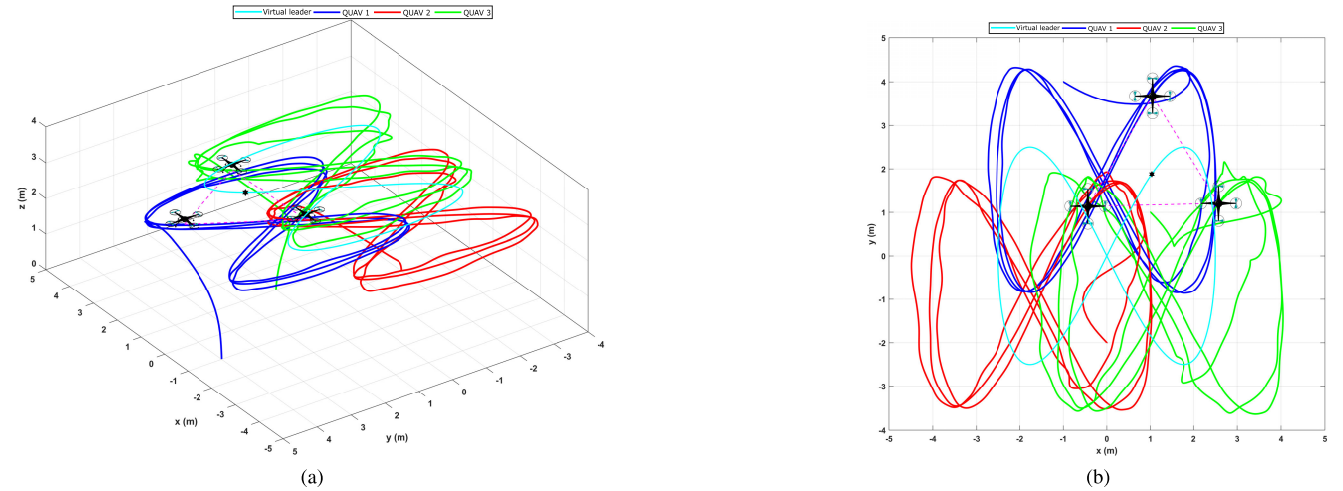

FIGURE 20. Results of the formation control of the DRFC method (a) Viewed in 3D (b) Viewed in 2D.

DRFC controllers. This confirms the outstanding property of fast convergence in finite time of our control system. On the other hand, Table 3 shows that our control system exhibits lower RMSE values compared to the PCFSMC and DRFC

TABLE 3. RMSE analysis.

Aircraft	Control method	Performance index RMSE		
		$e^x_{i,1}$	$e^y_{i,1}$	$e^z_{i,1}$
QUAV 1	DRFC	0.406	0.138	0.394
	PCFSMC	0.409	0.156	0.374
	Proposed	0.251	0.093	0.216
QUAV 2	DRFC	0.161	0.159	0.391
	PCFSMC	0.172	0.170	0.374
	Proposed	0.097	0.102	0.215
QUAV 3	DRFC	0.138	0.242	0.392
	PCFSMC	0.133	0.241	0.346
	Proposed	0.081	0.148	0.214

TABLE 4. Convergence time analysis.

Aircraft	Control method	Performance index Settling time		
		$e^x_{i,1}$	$e^y_{i,1}$	$e^z_{i,1}$
QUAV 1	DRFC	4.095	7.989	-
	PCFSMC	3.596	6.506	-
	Proposed	3.290	3.270	3.070
QUAV 2	DRFC	5.794	3.933	-
	PCFSMC	4.056	3.180	-
	Proposed	2.540	2.940	3.070
QUAV 3	DRFC	4.069	7.989	-
	PCFSMC	3.095	6.540	-
	Proposed	2.080	3.310	3.060

controllers. This confirms the remarkable robustness and tracking accuracy property of our control system. Overall, the quantitative results obtained in Tables 2 and 3 verify the superiority of our control method proposed in this research regarding fast convergence in finite time, tracking accuracy, and robustness.

B. FLIGHT SCENARIO 2

For further evaluation of the robustness and adaptability capabilities of the proposed control system, this flight scenario simulates the entry of the QUAVs into a windy area with more realistic wind speeds than in the previous scenario. In addition, uncertainties of unmodeled internal dynamics and variations of aircraft physical parameters are considered. This approach reflects practical conditions where all these large lumped uncertainties simultaneously affect the aircraft dynamics. For this purpose, lumped uncertainties are defined as:

a) External disturbances: Suppose that the QUAVs enter a windy area with wind speeds that can reach a velocity of 8m/s, as shown in Figure 13. For this purpose, the Dryden wind model is considered an external disturbance in this flight scenario [48]. Therefore, the components of $d^{\text{ext}}_{i,\xi}$ along the three axes are expressed as:

$$\begin{cases} d^{\text{ext}}_{i,x} = -K_{d,x}(\dot{x}_i - W_x)^2 \,\text{sign}(\dot{x}_i - W_x) \text{ m/s}^2, \\ d^{\text{ext}}_{i,y} = -K_{d,y}(\dot{y}_i - W_y)^2 \,\text{sign}(\dot{y}_i - W_y) \text{ m/s}^2, \\ d^{\text{ext}}_{i,z} = -K_{d,z}(\dot{z}_i - W_z)^2 \,\text{sign}(\dot{z}_i - W_z) \text{ m/s}^2. \end{cases} \tag{64}$$

where $K_{d,x}, K_{d,y}, K_{d,z} \in \mathbb{R}^+$. The terms W_x, W_y, W_z represent the total wind speeds along the three axes. **b) Internal uncertainties: b1) Modeling uncertainties:** Similar to the modeling uncertainties of the previous scenario. **b2) Parametric uncertainties:** For this flight scenario, parametric uncertainties of +30% on the mass and moments of inertia are considered.

The initial positional conditions of the three QUAVs are configured as $\xi_1(0) = [-1, 4, 0.01]^T$m, $\xi_2(0) = [0.01, -2, 0.01]^T$m, $\xi_3(0) = [1, 1, 0.01]^T$m. The initial velocities of the three aircraft are set to zero. The following Cartesian trajectory is established for the virtual leader:

$$\xi_0 = [x_0, y_0, z_0]^T = [2.5\cos(0.2t), 2.5\sin(0.4t,), 3]^T \text{m}. \tag{65}$$

The results for this scenario are presented in Figures 14-17. The temporal position and linear velocity response of the three QUAVs are shown in Figures 14 and 15, respectively. These figures reveal that, despite being subject to realistic wind gusts and internal uncertainties, the proposed RFDCFCP approach allows the aircraft to reach the desired formation quickly. Furthermore, it can be observed that the aircraft achieves a consensus, maintaining the desired formation satisfactorily while following the reference Cartesian trajectory. The temporal attitude response of the QUAVs is presented in Figure 16, where it is noticed that the proposed RFASC approach allows tracking the attitude angles stably, adjusting to the desired attitude generated by the RFDCFCP. The four control inputs of the three QUAVs are presented in Figure 17.

The comparison results of our proposed control system with the PCFSMC and DRFC methods are presented in Figures 18-23. Figure 18 shows the flight formation of the three QUAVs in 3D and 2D under our proposed control system. As in the previous scenario, our proposed method achieves and maintains the desired formation pattern stably throughout the flight mission, with accurate tracking of the reference Cartesian trajectory. In comparison, the PCFSMC control method, although maintaining the desired formation pattern, demonstrates to be sensitive to large lumped uncertainties. This is evidenced in Figure 19, where wind gusts and internal uncertainties clearly affect the control performance of the QUAVs, resulting in a loss of accuracy in tracking the reference Cartesian trajectory. On the other hand, the DRFC control method is the most affected in this comparison. This controller demonstrates low robustness and lower tracking accuracy, as seen in Figure 20. Overall, the proposed formation control system demonstrates its superiority in robustness and adaptability, unlike the PCFSMC and DRFC methods, which exhibit more noticeable deviations and fluctuations in their formation, especially visible in the 2D flight formation in Figures 19(b) and 20(b).

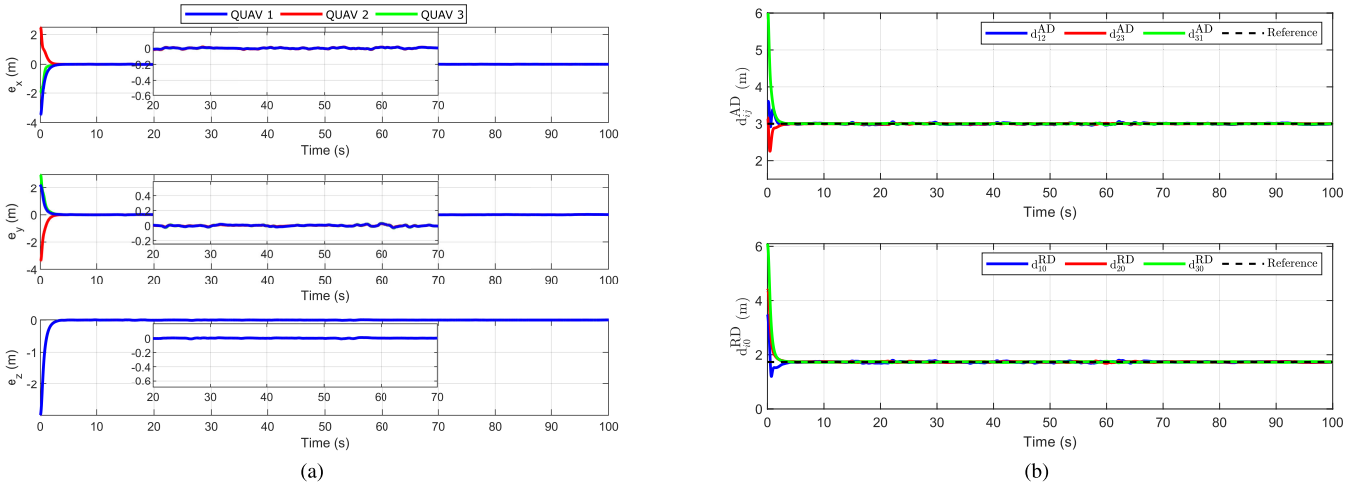

FIGURE 21. Results of the proposed method: (a) Formation errors (b) Adjacent and relative distances.

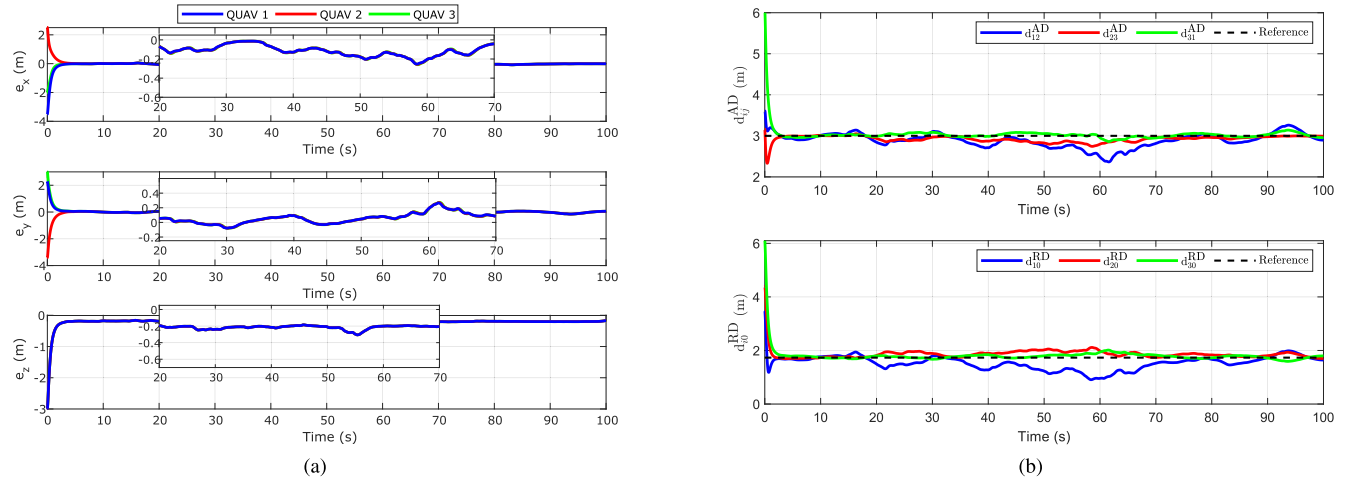

FIGURE 22. Results of the PCFSMC method: (a) Formation errors (b) Adjacent and relative distances.

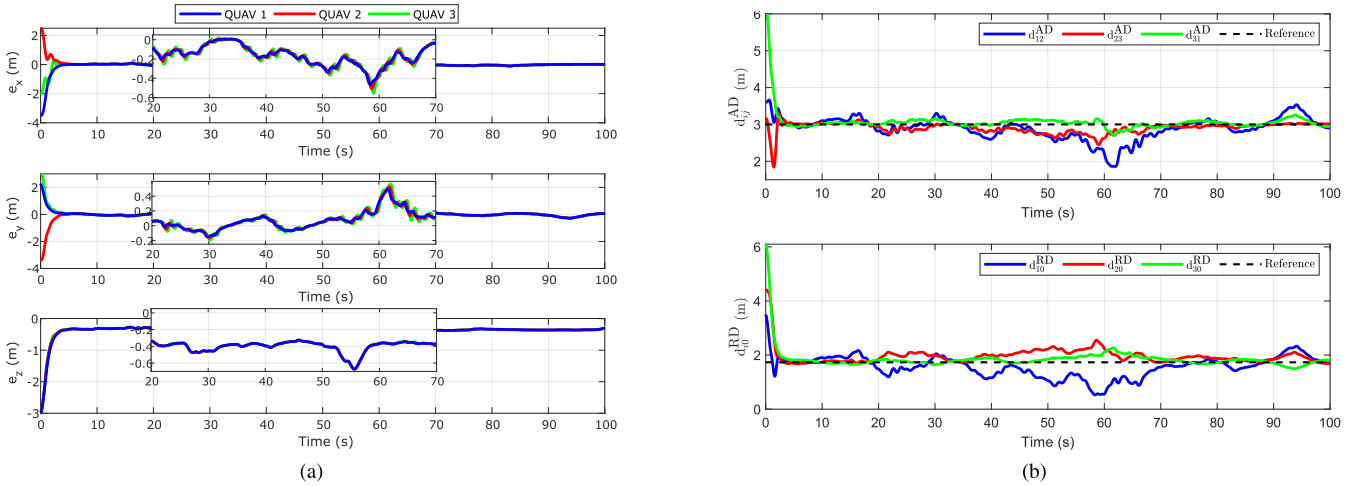

FIGURE 23. Results of the DRFC method: (a) Formation errors (b) Adjacent and relative distances.

The formation tracking errors, adjacent distances, and relative distances for this flight scenario under the three formation controllers are presented in Figures 21, 22, and 23, respectively. Figure 21(a) highlights that the formation

TABLE 5. RMSE analysis.

Aircraft	Control method	Performance index RMSE		
		$e^x_{i,1}$	$e^y_{i,1}$	$e^z_{i,1}$
QUAV 1	DRFC	0.408	0.248	0.497
	PCFSMC	0.395	0.377	0.383
	Proposed	0.249	0.161	0.215
QUAV 2	DRFC	0.288	0.383	0.492
	PCFSMC	0.282	0.373	0.385
	Proposed	0.168	0.249	0.215
QUAV 3	DRFC	0.265	0.328	0.491
	PCFSMC	0.245	0.332	0.389
	Proposed	0.147	0.209	0.215

tracking errors of our proposed control system achieve faster convergence to zero and consistently remain close to the origin neighborhood despite realistic wind gusts, modeling uncertainties, and variations of aircraft physical parameters. This demonstrates that the desired formation pattern has been successfully maintained without any geometric deformation, as seen in the 3D flight formation in Figure 18. This behavior is supported by observing that the adjacent distances and relative distances of the three QUAVs in Figure 21(b) rapidly converge to their desired values of 3 meters and 1.73 meters, respectively, and remain constant throughout the flight formation. In contrast, the PCFSMC and DRFC methods show that the formation tracking errors (see Figures 22(a) and 23(a), respectively) are inevitably affected by the large lumped uncertainties, experiencing more significant fluctuations and deviations. Looking at the zoomed regions in the interval [20-80]s, it can be seen that the errors of these control methods do not remain close to the neighborhood of the origin, indicating that the desired formation pattern has not been satisfactorily maintained and geometrical deformations have occurred. This is evidenced by looking at the adjacent distances and relative distances of the PCFSMC and DRFC methods in Figures 22(b) and 23(b), along with their 3D flight formation in Figures 19 and 20, respectively.

The settling time and RMSE performance indices are calculated for each control method and presented in Tables 4 and 5 to provide a quantitative comparison of the obtained results. Table 4 shows that our proposed control system exhibits lower convergence times in all formation tracking errors compared to the PCFSMC and DRFC control methods. This confirms the outstanding finite-time fast convergence property of our control system. Moreover, in Table 5, it is observed that our control system exhibits lower RMSE values compared to the PCFSMC and DRFC controllers, which ratifies the remarkable robustness and high tracking accuracy of our control system. Overall, the quantitative results obtained in Tables 4 and 5 verify the superiority of our control strategy proposed in this research regarding fast convergence in finite time, tracking accuracy, and robustness in a complex and challenging flight scenario with realistic wind gusts and large internal uncertainties.

VII. CONCLUSION AND FUTURE WORK

In this research, a distributed robust control system has been designed to address the flight formation control of a multi-QUAV system in complex and challenging flight scenarios with large lumped uncertainties. For this purpose, a novel nonlinear control strategy, ABRINFTSMC, has been designed. Based on this proposed strategy, an RFDCFCP has been developed for the underactuated position subsystem, and for the fully actuated attitude subsystem, an RFASC has been developed. The effectiveness of the proposed method has been verified by numerical simulations and compared with recent formation control methods.

The obtained results have demonstrated the outstanding capability of our proposed control system to quickly achieve and consistently maintain the desired formation pattern throughout the flight mission, even in challenging environments with the presence of realistic wind gusts, unmodeled internal dynamics, and varying physical parameters of the QUAVs. By performing quantitative comparative analysis with PCFSMC and DRFC works, the superiority of our proposed control method in terms of fast convergence in finite time, tracking accuracy, and robustness has been evidenced.

In future works, we include the practical implementation of the proposed control system for formation control with DJI-F450 physical aircraft in a real flight environment. In addition, we plan to implement the proposed method for the cooperative transport of suspended payloads.

ACKNOWLEDGMENT

The authors would like to thank the Instituto de Investigación Astronómico y Aeroespacial Pedro Paulet (IAAPP), UNSA, for making this research possible.

REFERENCES

[1] K. Mohammadi, S. Sirouspour, and A. Grivani, "Control of multiple quad-copters with a cable-suspended payload subject to disturbances," *IEEE/ASME Trans. Mechatronics*, vol. 25, no. 4, pp. 1709–1718, Aug. 2020.

[2] J. Geng and J. W. Langelaan, "Cooperative transport of a slung load using load-leading control," *J. Guid., Control, Dyn.*, vol. 43, no. 7, pp. 1313–1331, Jul. 2020.

[3] R. I. Mukhamediev, K. Yakunin, M. Aubakirov, I. Assanov, Y. Kuchin, A. Symagulov, V. Levashenko, E. Zaitseva, D. Sokolov, and Y. Amirgaliyev, "Coverage path planning optimization of heterogeneous UAVs group for precision agriculture," *IEEE Access*, vol. 11, pp. 5789–5803, 2023.

[4] C. Ju and H. I. Son, "Multiple UAV systems for agricultural applications: Control, implementation, and evaluation," *Electronics*, vol. 7, no. 9, p. 162, Aug. 2018.

[5] L. Xing, X. Fan, Y. Dong, Z. Xiong, L. Xing, Y. Yang, H. Bai, and C. Zhou, "Multi-UAV cooperative system for search and rescue based on YOLOv5," *Int. J. Disaster Risk Reduction*, vol. 76, Jun. 2022, Art. no. 102972.

[6] J. P. Queralta, J. Taipalmaa, B. C. Pullinen, V. K. Sarker, T. N. Gia, H. Tenhunen, M. Gabbouj, J. Raitoharju, and T. Westerlund, "Collaborative multi-robot search and rescue: Planning, coordination, perception, and active vision," *IEEE Access*, vol. 8, pp. 191617–191643, 2020.

[7] M. Idrissi, M. Salami, and F. Annaz, "A review of quadrotor unmanned aerial vehicles: Applications, architectural design and control algorithms," *J. Intell. Robotic Syst.*, vol. 104, no. 2, p. 22, Feb. 2022.

[8] B. Tian, H. Lu, Z. Zuo, Q. Zong, and Y. Zhang, "Multivariable finite-time output feedback trajectory tracking control of quadrotor helicopters," *Int. J. Robust Nonlinear Control*, vol. 28, no. 1, pp. 281–295, Jan. 2018.

[9] B. J. Emran and H. Najjaran, "A review of quadrotor: An underactuated mechanical system," *Annu. Rev. Control*, vol. 46, pp. 165–180, Jan. 2018.

[10] Q. Quan, *Introduction to Multicopter Design and Control*. Berlin, Germany: Springer, 2017.

[11] R. Mahony, V. Kumar, and P. Corke, "Multirotor aerial vehicles: Modeling, estimation, and control of quadrotor," *IEEE Robot. Autom. Mag.*, vol. 19, no. 3, pp. 20–32, Sep. 2012.

[12] O. Mechali, L. Xu, Y. Huang, M. Shi, and X. Xie, "Observer-based fixed-time continuous nonsingular terminal sliding mode control of quadrotor aircraft under uncertainties and disturbances for robust trajectory tracking: Theory and experiment," *Control Eng. Pract.*, vol. 111, Jun. 2021, Art. no. 104806.

[13] L. Martins, C. Cardeira, and P. Oliveira, "Global trajectory tracking for quadrotors: An MRP-based hybrid strategy with input saturation," *Automatica*, vol. 162, Apr. 2024, Art. no. 111521.

[14] L. F. C. Ccari and P. R. Yanyachi, "A novel neural network-based robust adaptive formation control for cooperative transport of a payload using two underactuated quadcopters," *IEEE Access*, vol. 11, pp. 36015–36028, 2023.

[15] D. Shen and Q. Lu, "Hierarchical formation control with applications to multi-quadrotor systems," *IEEE Access*, vol. 7, pp. 130599–130609, 2019.

[16] O. Mechali, L. Xu, and X. Xie, "Nonlinear homogeneous sliding mode approach for fixed-time robust formation tracking control of networked quadrotors," *Aerosp. Sci. Technol.*, vol. 126, Jul. 2022, Art. no. 107639.

[17] Q. Li, Y. Chen, and K. Liang, "Predefined-time formation control of the quadrotor-UAV cluster' position system," *Appl. Math. Model.*, vol. 116, pp. 45–64, Apr. 2023.

[18] K. U. Lee, Y. H. Choi, and J. B. Park, "Backstepping based formation control of quadrotors with the state transformation technique," *Appl. Sci.*, vol. 7, no. 11, p. 1170, Nov. 2017.

[19] H. Liu, T. Ma, F. L. Lewis, and Y. Wan, "Robust formation control for multiple quadrotors with nonlinearities and disturbances," *IEEE Trans. Cybern.*, vol. 50, no. 4, pp. 1362–1371, Apr. 2020.

[20] J. Wang, X. Ma, H. Li, and B. Tian, "Self-triggered sliding mode control for distributed formation of multiple quadrotors," *J. Franklin Inst.*, vol. 357, no. 17, pp. 12223–12240, Nov. 2020.

[21] N. Alabsari, A.-W.-A. Saif, S. El-Ferik, S. Duffuaa, and N. Derbel, "Cooperative flight control of a fleet of quadrotors using fractional sliding mode with potential field algorithms," *IEEE Access*, vol. 12, pp. 24525–24543, 2024.

[22] D.-N. Bui and M. D. Phung, "Radial basis function neural networks for formation control of unmanned aerial vehicles," *Robotica*, pp. 1–19, Apr. 2024, doi: 10.1017/S0263574724000559.

[23] Y. Fei, P. Shi, C. P. Lim, and X. Yuan, "Finite-time observer-based formation tracking with application to omnidirectional robots," *IEEE Trans. Ind. Electron.*, vol. 70, no. 10, pp. 10598–10606, Oct. 2023.

[24] B. Ning and Q.-L. Han, "Prescribed finite-time consensus tracking for multiagent systems with nonholonomic chained-form dynamics," *IEEE Trans. Autom. Control*, vol. 64, no. 4, pp. 1686–1693, Apr. 2019.

[25] B. Huang, S. Song, C. Zhu, J. Li, and B. Zhou, "Finite-time distributed formation control for multiple unmanned surface vehicles with input saturation," *Ocean Eng.*, vol. 233, Aug. 2021, Art. no. 109158.

[26] M. Fu and L. Yu, "Finite-time extended state observer-based distributed formation control for marine surface vehicles with input saturation and disturbances," *Ocean Eng.*, vol. 159, pp. 219–227, Jul. 2018.

[27] L. Dou, S. Cai, X. Zhang, X. Su, and R. Zhang, "Event-triggered-based adaptive dynamic programming for distributed formation control of multi-UAV," *J. Franklin Inst.*, vol. 359, no. 8, pp. 3671–3691, May 2022.

[28] Y. Li, M. Jiu, Q. Sun, and Q. Dong, "An adaptive distributed consensus control algorithm based on continuous terminal sliding model for multiple quad rotors' formation tracking," *IEEE Access*, vol. 7, pp. 173955–173967, 2019.

[29] J. Wang, L. Han, X. Dong, Q. Li, and Z. Ren, "Distributed sliding mode control for time-varying formation tracking of multi-UAV system with a dynamic leader," *Aerosp. Sci. Technol.*, vol. 111, Apr. 2021, Art. no. 106549.

[30] H. Du, W. Zhu, G. Wen, and D. Wu, "Finite-time formation control for a group of quadrotor aircraft," *Aerosp. Sci. Technol.*, vol. 69, pp. 609–616, Oct. 2017.

[31] Y. Huang, W. Liu, B. Li, Y. Yang, and B. Xiao, "Finite-time formation tracking control with collision avoidance for quadrotor UAVs," *J. Franklin Inst.*, vol. 357, no. 7, pp. 4034–4058, May 2020.

[32] W. Zhang, C. Dong, M. Ran, and Y. Liu, "Fully distributed time-varying formation tracking control for multiple quadrotor vehicles via finite-time convergent extended state observer," *Chin. J. Aeronaut.*, vol. 33, no. 11, pp. 2907–2920, Nov. 2020.

[33] N. P. Nguyen, D. Park, D. N. Ngoc, N. Xuan-Mung, T. T. Huynh, T. N. Nguyen, and S. K. Hong, "Quadrotor formation control via terminal sliding mode approach: Theory and experiment results," *Drones*, vol. 6, no. 7, p. 172, Jul. 2022.

[34] I. H. Imran, D. F. Kurtulus, A. M. Memon, S. Goli, T. Kouser, and L. M. Alhems, "Distributed robust formation control of heterogeneous multi-UAVs with disturbance rejection," *IEEE Access*, vol. 12, pp. 55326–55341, 2024.

[35] M. Khodaverdian, S. Hajshirmohamadi, A. Hakobyan, and S. Ijaz, "Predictor-based constrained fixed-time sliding mode control of multi-UAV formation flight," *Aerosp. Sci. Technol.*, vol. 148, May 2024, Art. no. 109113.

[36] F. Wang, B. Chen, X. Liu, and C. Lin, "Finite-time adaptive fuzzy tracking control design for nonlinear systems," *IEEE Trans. Fuzzy Syst.*, vol. 26, no. 3, pp. 1207–1216, Jun. 2018.

[37] L. Sun and Y. Liu, "Extended state observer augmented finite-time trajectory tracking control of uncertain mechanical systems," *Mech. Syst. Signal Process.*, vol. 139, May 2020, Art. no. 106374.

[38] H. J. Brascamp and E. H. Lieb, "Best constants in Young's inequality, its converse, and its generalization to more than three functions," *Adv. Math.*, vol. 20, no. 2, pp. 151–173, May 1976.

[39] N.-N. Zhao, L.-B. Wu, X.-Y. Ouyang, Y. Yan, and R.-Y. Zhang, "Finite-time adaptive fuzzy tracking control for nonlinear systems with disturbances and dead-zone nonlinearities," *Appl. Math. Comput.*, vol. 362, Dec. 2019, Art. no. 124494.

[40] G. Hardy, J. Littlewood, and G. Pólya, *Inequalities*. Cambridge, U.K.: Cambridge Univ. Press, 1952.

[41] F. Chen, R. Jiang, K. Zhang, B. Jiang, and G. Tao, "Robust backstepping sliding-mode control and observer-based fault estimation for a quadrotor UAV," *IEEE Trans. Ind. Electron.*, vol. 63, no. 8, pp. 5044–5056, Aug. 2016.

[42] O. Mechali, L. Xu, X. Xie, and J. Iqbal, "Fixed-time nonlinear homogeneous sliding mode approach for robust tracking control of multirotor aircraft: Experimental validation," *J. Franklin Inst.*, vol. 359, no. 5, pp. 1971–2029, Mar. 2022.

[43] V. K. Tripathi, A. K. Kamath, L. Behera, N. K. Verma, and S. Nahavandi, "An adaptive fast terminal sliding-mode controller with power rate proportional reaching law for quadrotor position and altitude tracking," *IEEE Trans. Syst., Man, Cybern., Syst.*, vol. 52, no. 6, pp. 3612–3625, Jun. 2022.

[44] H. Rios, R. Falcon, O. A. Gonzalez, and A. Dzul, "Continuous sliding-mode control strategies for quadrotor robust tracking: Real-time application," *IEEE Trans. Ind. Electron.*, vol. 66, no. 2, pp. 1264–1272, Feb. 2019.

[45] C.-S. Chiu, "Derivative and integral terminal sliding mode control for a class of MIMO nonlinear systems," *Automatica*, vol. 48, no. 2, pp. 316–326, Feb. 2012.

[46] K. Shao, J. Zheng, K. Huang, H. Wang, Z. Man, and M. Fu, "Finite-time control of a linear motor positioner using adaptive recursive terminal sliding mode," *IEEE Trans. Ind. Electron.*, vol. 67, no. 8, pp. 6659–6668, Aug. 2020.

[47] M. Labbadi and M. Cherkaoui, "Robust adaptive nonsingular fast terminal sliding-mode tracking control for an uncertain quadrotor UAV subjected to disturbances," *ISA Trans.*, vol. 99, pp. 290–304, Apr. 2020.

[48] K. Eliker and W. Zhang, "Finite-time adaptive integral backstepping fast terminal sliding mode control application on quadrotor UAV," *Int. J. Control, Autom. Syst.*, vol. 18, no. 2, pp. 415–430, Feb. 2020.

LUIS F. CANAZA CCARI received the B.Sc. degree in electronic engineering from the Universidad Nacional de San Agustín de Arequipa (UNSA), Peru, in 2021. From 2022 to 2023, he was a Research Assistant in a project funded by CONCYTEC-Peru. He is a RENACYT Researcher currently working as a Research Assistant with the Pedro Paulet Aerospace and Astronomy Research Institute (IAAPP), UNSA. His research interests include autonomous robotics, advanced nonlinear control, system modeling, control of quadcopters, robotic manipulators, and multi-agent systems.

PABLO RAUL YANYACHI (Senior Member, IEEE) received the M.Sc. degree in automatic control from the Polytechnic Institute of Leningrad and the Ph.D. degree in electrical engineering from the Polytechnic School, University of São Paulo, Brazil. He is currently a main Professor with the Department of Electronic Engineering, Universidad Nacional de San Agustín de Arequipa (UNSA). He is the Station Manager of the Nasa Laser Tracking Station TLRS-3, Arequipa, Peru. He is also the Director of Instituto de Investigación Astronómico y Aeroespacial Pedro Paulet (IAAPP), UNSA.

JUAN C. CUTIPA LUQUE (Member, IEEE) was born in Arequipa, Peru. He received the degree in electronic engineering from the Universidad Nacional de San Agustín de Arequipa, in 2004, and the M.Sc. and Ph.D. degrees in mechanical engineering from the University of São Paulo, Brazil, in 2007 and 2012, respectively. He is currently a Professor with the Department of Electronic Engineering, Universidad Nacional de San Agustín de Arequipa. His research interests include advanced control systems for autonomous underwater vehicles (AUVs), remote-operated submersible vehicles (ROVs), unmanned surface vehicles (USV), and electric vehicles.

DANIEL YANYACHI was born in Peru. He received the M.Sc. and Ph.D. degrees in electrical engineering from the Leningrad Polytechnic Institute. He has lectured for many years as a Full Professor with the Department of Electronic Engineering, Universidad Nacional de San Agustín de Arequipa, Peru. His research interests include processing control systems, mining, manufacturing, and complex and advanced control systems.